Sub–continental lithospheric mantle beneath the Adamawa volcanic area (Cameroon Volcanic Line): inference from lavas and hosted mantle xenoliths from Bini Warack, NE-Ngaoundéré, Cameroon (Central Africa).

Manteau lithosphérique sous-continental sous la zone volcanique de l'Adamaoua (Ligne Volcanique du Cameroun): inférence à partir des laves et xénolithes mantelliques de Bini Warack, NE-Ngaoundéré, Cameroun (Afrique centrale).

Benoît Joseph Mbassa *[1], Olivier Vanderhaeghe [2], Michel Gregoire [2], Mathieu Benoît [2], Zenon Itiga [3], Caroline Ngwa Neh[1] , Pierre Kamgang [4]

[1] Institute of Geological and Mining Research, PO Box 4110, Yaoundé, Cameroon

[2] GET-OMP, Université de Toulouse, UPS, CNRS, IRD, CNES, 14 avenue E. Belin, 31400 Toulouse, France

[3] Département des Sciences de la Terre, Faculté des Sciences, Université de Douala, PO Box 24157 Douala, Cameroon

[4] Département des Sciences de la Terre, Faculté des Sciences, Université de Yaoundé I, BP 812 Yaoundé, Cameroon,

Corresponding author E-mail: benjo_mbassa@yahoo.fr

Abstract

The sub continental lithospheric mantle (SCLM) beneath the Cameroon volcanic line (CVL) is vertically and laterally heterogenous, consisting of a complex mixing of DMM, HIMU and EM1, affected by modal or cryptic metasomatism, depending on the area. The petrography, whole rock geochemical data as well as minerals chemical composition of lavas and mantle xenoliths from Bini Warack area combined with Sr isotope compositions provide constraints on the origin and thermochemical evolution of the SCLM beneath this sector of the CVL. The host lavas are basanite, basalt and latite with OIB affinity, characterized by moderate to high

This provisional PDF is the accepted version. The article should be cited as: BSGF - Earth Sciences Bulletin, https://doi.org/10.1051/bsgf/2026005

silica and alkali contents (SiO_2 = 42.35 – 56.56 wt %, K_2O+Na_2O = 2.34 – 7.07 wt %), a high Ba/Rb ranging from 12.2 to 26.1, a low Rb/Sr from 0.03 to 0.08, strong enrichment in LREE relative to HREE (La_N/Yb_N: 9.3 – 30), and moderately enriched in radiogenic isotopes (e.g., 0.702987 < $^{87}Sr/^{86}Sr_{initial}$ < 0.703206; 0.512854 < $^{143}Nd/^{144}Nd_{initial}$ < 0.512918) with positive $\varepsilon Nd_{initial}$ (+4.84 – +6.09). These features are consistent with an origin of the lavas by low degree of partial melting (< 2%) of a lherzolitic mantle source containing 2 to 6% garnet. These lavas have then evolved by fractional crystallization without any evidence of crustal contamination. The studied mantle xenoliths are spinel–bearing lherzolites, characterized by U/Th ratios typically lower than 1, a slight enrichment in LILE relative to HFSE, and mainly consist of minerals with fertile composition (Fo_{84-91}; spinel Cr#:0.1 – 0.22; Al–rich pyroxenes). They are consistent with refractory mantle peridotite that evidenced low partial–melting degrees. Trace element concentrations of host lavas (high Ba/Rb: 12.2 – 26.1 and low Rb/Sr: 0.03 – 0.08) together with olivine's crystals chemical features (high Ca/Fe and 100*Mn/Fe ratios; low 100*Ni/Mg ratios) and low Ca/Al ratios (< 5) of clinopyroxenes in spinel-bearing lherzolites xenoliths suggest that the SCLM beneath the Bini Warack area is likely a juvenile lithospheric mantle which has undergone a carbonate–rich metasomatism.

Keywords: Cameroon Volcanic Line - OIB affinity - mantle xenoliths - spinel lherzolites - low partial melting degrees - Carbonate metasomatism

Résumé

Le manteau lithosphérique sous-continental (MLSC) sous la ligne volcanique du Cameroun (LVC) est verticalement et latéralement hétérogène, constitué d'un mélange complexe de DMM, HIMU et EM1, affecté par un métasomatisme modal ou cryptique selon la zone. La pétrographie, les données géochimiques des roches totales ainsi que la composition chimique des minéraux des laves et des xénolithes mantelliques de la région de Bini Warack, combinées aux compositions isotopiques Sr, fournissent des informations sur l'origine et l'évolution thermochimique du MLSC sous ce secteur de la LVC.

Les laves hôtes ont des compositions de basanite, basalte et de latite présentant des affinités avec les OIB, et caractérisées par i) des teneurs modérées à élevées en silice et en alcalins (SiO_2 = 42,35 – 56,56 %, K_2O+Na_2O = 2,34 – 7,07 %), ii) de forts rapports Ba/Rb (12,2 – 26,1), iii) de faibles rapports Rb/Sr (0,03 – 0,08), iv) un fort enrichissement en terres rares légères par rapport aux terres rares lourdes (La_N/Yb_N : 9,3 – 30), et v) un enrichissement modéré en isotopes radiogéniques (0.702987 < $^{87}Sr/^{86}Sr_{initial}$ < 0.703206 ; 0.512854 < $^{143}Nd/^{144}Nd_{initial}$ < 0.512918) marqué par des εNd initiaux positifs (+4.84 – +6.09). Ces caractéristiques sont compatibles avec une origine des laves par un faible degré de fusion partielle (moins de 2 %) d'un manteau à lherzolite contenant 2 à 6 % de grenat. Les laves de Bini Warack ont ensuite évolué par cristallisation fractionnée sans trace de contamination crustale.

Les xénolithes quant à eux sont des lherzolites à spinelle, caractérisés par des rapports U/Th généralement inférieurs à 1, un léger enrichissement en LILE par rapport aux HFSE et principalement constitués de minéraux de composition fertile (Fo_{84-91} ; spinelle Cr# : 0,1 - 0,22 ; pyroxènes alumineux). Ces xénolithes sont compatibles avec un manteau péridotitique réfractaire ayant subi de faibles degrés de fusion partielle.

*Les teneurs en éléments traces des laves hôtes (Ba/Rb élevé : 12,2 - 26,1 et Rb/Sr faible : 0,03 - 0,08), les caractéristiques chimiques des cristaux d'olivine (rapports Ca/Fe et 100*Mn/Fe élevés ; ainsi que les faibles rapports 100*Ni/Mg et Ca/Al <5) des clinopyroxènes des lherzolites étudiées, suggèrent que le MLSC sous la zone de Bini Warack est sans doute un manteau lithosphérique juvenile ayant subi un métasomatisme carbonaté.*

Mots-clés: Ligne volcanique du Cameroun - affinité OIB - xénolites manteliques - lherzolites à spinelle – faibles degrés de fusion partielle - métasomatisme carbonatée

1. Introduction.

Alkaline mafic to ultramafic volcanic rocks have been studied worldwide because they generally host mantle xenoliths that provide insights on the composition of the upper mantle.

The mantle fragments found in volcanic areas emplaced within Archean and Paleoproterozoic belts have been considered to have temporal and genetic relationship with the overlying crust (Carlson et al., 2005) while in younger terranes and oceanic settings, this correlation remains unclear (Liu et al., 2015, and references therein). The chemical diversity of continental intraplate magmas has been attributed to the heterogeneity of the mantle sources (Stracke et al., 2005 and references therein) and/or to interactions between an upwelling plume with the lithospheric mantle or the upper crust (MacDonald et al., 2001; Lundstrom et al., 2003; Yokoyama et al., 2007). The sub–continental lithospheric mantle (SCLM) is one of the Earth reservoirs representing about 2.5 vol.% of the whole mantle, where basaltic magmas are generated by direct melting (Hawkesworth et al., 1983) or through delamination of this lithosphere and re–incorporation of the convecting mantle (McKenzie & O'Nions 1983, 1995). The SCLM underlying some continental domains generally displays features of OIB– mantle source and consists of lherzolites (Downes et al., 2003). The composition of the SCLM is known from the study of either mantle xenoliths hosted in alkaline basalts, or more rarely that of massive peridotites found in areas having undergone significant tectonic activity such as Lherz in the southern France. However, samples from both settings provide disrupted information on the SCLM due either to their interaction with the host magma in the case of mantle xenoliths or to wide serpentinization and interaction with crustal fluids during their emplacement in the case of massifs (Pearson & Nowell, 2002). Accordingly, characterizing the SCLM is crucial to understand crustal growth and stabilization, preservation and transformation of continents through time (Lin et al., 2022).

In this contribution, we present a set of new field, mineralogical, petrographic, whole–rock geochemical, and Sr–Nd isotopic data on peridotite xenoliths together with their basaltic host lavas from Bini Warack in the Eastern Ngaoundéré area in order to characterize the regional SCLM beneath the Adamawa plateau, discuss its origin and evolution, and explore the possible links with the growth and differentiation of the overlying Precambrian crust.

2. Geological context

The Cameroon Volcanic Line (CVL) is a 1600 km Y–shaped intracontinental mainly alkaline volcanic structure straddling the continent– ocean boundary, where the volcanic activity is due to instability within the subcontinental lithospheric mantle at the continental edge (Milelli et al., 2012). The magmas have been proposed to originate either from an asthenospheric source or an enriched SCLM, without significant interaction with the overlying crusts (Marzoli et al., 2000, Rankenburg et al., 2005, Déruelle et al., 2007). Volcanic rocks are typically SiO_2-undersaturated in the oceanic sector, mainly basaltic at the continent–ocean boundary with the exception of Mt Etinde that entirely consists of feldspathoids–rich lavas, then generally bimodal in the continental massifs, with abundant mafic and felsic lavas and with few intermediate terms.

The Ngaoundéré volcanic district which includes our study area is the easternmost area of the CVL (Fig. 1). The volcanic activity dated between Oligocene and Pleistocene (Temdjim et al., 2004, Itiga et al., 2013) is characterized by the presence of numerous and diverse eruptive centers including lava flows, cones, plugs and maars respectively associated with effusive and hydro–magmatic explosive dynamisms (Temdjim et al., 2006, Nkouandou et al., 2008, Tiabou et al., 2019). Several studies based on xenoliths from Ngaoundéré volcanic district (Nkouandou & Temdjim, 2011, Nguihdama et al., 2014, Nkouandou et al., 2015, Adama et al., 2021, Wagsong Njombié et al., 2018) provide significant informations on the nature and the evolution of the lithosphere beneath. The mantle xenoliths of this volcanic district consist of lherzolite, harzburgite and olivine websterite in Ngaoundéré (Nkouandou et al., 2015), harzburgite in Lake Guinnadji and Ngao Djalsoka (Adama et al., 2021), spinel–bearing lherzolite in Hosséré Garba (Nguihdama et al., 2014), Ngao Voglar (Nkouandou & Temdjim, 2011) and Youkou (Wagson Njombié et al., 2018). These xenoliths have been interpreted to represent refractory mantle residues after partial melting that have likely experienced refertilization processes. According to their equilibrium temperatures and corresponding pressures, xenoliths from the Adamawa region have been entrained from depths range of 25–85 km (Nkouandou & Temdjim, 2011, Nkouandou et al., 2015) involving

a limited asthenosphere upwelling. Metasomatic processes probably induced by plume–related hydrous silicate melts have been locally recorded and invoked to explain secondary enrichment in some highly incompatible trace elements (Wagsong Njombié et al., 2018, Adama et al., 2021). Overall, the SCLM beneath the CVL is likely both vertically and laterally heterogenous (Pintér et al., 2015).

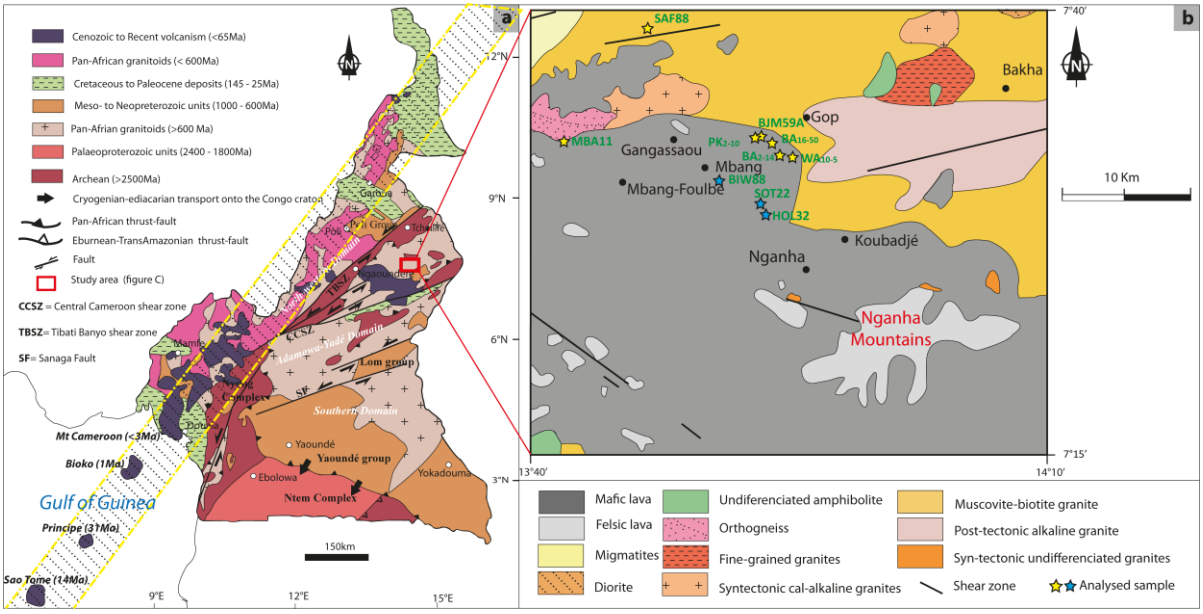

Figure 1: Location of the study area: (a) Geological sketch of Cameroon (modified after Ngako et al., 2003; Owona et al., 2013) with position of the study area; (b) Simplified geological map of the study area (modified from Mbassa et al., 2015). The hatched band outlined by dashed yellow lines represents the CVL. The blue stars represent lava enclosing mantle xenoliths.

3. Samples processing and analytical methods

12 samples from Bini Warak area, located NE of Ngaoundéré (Cameroon) including 6 mafic lavas and 6 mantle xenoliths have been selected for the geochemical analyses. However, these analyses have are supplemented by a certain number of published data from Tiabou et al (2019) for a better discussion. Powders and thin sections of selected rock samples were prepared at the laboratory *Geosciences Environnement Toulouse* (GET) of the *CNRS*-

159 *CNES-IRD-Université de Toulouse* (France) for geochemical and mineralogical analyses.
160 Approximately 200 to 500 g of each sample were milled in a steel jaw crusher and then
161 pulverized in an agate mortar, for whole–rock geochemical and isotopic analysis. Whole–
162 rock major and trace elements concentrations have been determined at the *Service*
163 *d'Analyses des Roches et des Minéraux* (SARM–CRPG, Nancy, France) by ICP–OES and
164 ICP–MS respectively, following the procedure described in Carignan et al. (2001).
165 The minerals major elements analyses were carried out at the *Centre de*
166 *microcaractérisation Raimond Castaing* of the *CNRS–Université de Toulouse* (France) using
167 a Cameca SX Five electron microprobe. All analyzed samples were carbon coated (15 nm
168 thick layer, density 2.25 g/cm^3) before being introduced in the electron microprobe. The
169 analyses conditions were 15 kV accelerating voltage and 10 or 20 nA probe current
170 depending on the resistance of the mineral to the electron beam. The synthetic and natural
171 standards used for measurement of concentrations were: albite (Na), corundum (Al),
172 wollastonite (Si, Ca), sanidine (K), pyrophanite (Mn, Ti), hematite (Fe), periclase (Mg), Ni
173 metal (Ni), Cr_2O_3 (Cr) and reference zircon (Zr). The acquisition times for most analyzed
174 elements were 10 s at the peak and 5 s at either side of the peak for the continuous
175 background. The detection limits were 70 ppm for Cr and Zr and 100 ppm for Ni. The modal
176 proportion of minerals in lavas and xenoliths were determined using the *PetroMode*
177 spreadsheet (Christiansen, 2009) based on sample whole rock chemical composition and its
178 mineral phases. Minerals structural formulae were calculated using minerals spreadsheets
179 available on the GabbroSoft website at http://www.gabbrosoft.org/.
180 The Sr/Nd isotopic data were performed for 4 basanites at the GET laboratory, using the
181 Thermo Scientific TRITON+ solid source mass spectrometer, following Labou et al. (2020)
182 and Li et al. (2011, 2012) procedures. Before measurement, about 100 mg of whole rock
183 powder was weighed in a teflon beaker and dissolved in a 1:1 HF/HNO_3 mixture. After
184 dissolution, samples were diluted in 1 ml, 2% HNO_3 and Nd/Sr were extracted from the
185 matrix (2N HNO_3) using a combination of Sr–Spec and Thru–spec Eichrom resins. Mixed Sr
186 and REE were loaded on a Re filament and were run sequentially (first Sr then Nd) using a

187 double Re filament protocol. Interferences on ^{87}Rb and ^{144}Sm were monitored according to
188 the protocol of Li et al. (2012) and the quality and reproducibility of the measurements were
189 controlled using a sequential measurement of isotopic standards (SRM 987 and JNdi), doped
190 isotopic standards (NBS 987+ Rb and JNdi + Sm) and laboratory–dedicated Sr + REE
191 artificial solutions. Standard reproducibilities are $^{87}Sr/^{86}Sr$ = 0.710225, $^{143}Nd/^{144}Nd$ =
192 0.512509 and $^{145}Nd/^{144}Nd$ = 0.34897 for SRM–987 (pure and doped) and fall within the
193 recommended values. Measured blanks are 26 pg for Nd and 432 pg for Sr. $^{87}Sr/^{86}Sr$ and
194 $^{143}Nd/^{144}Nd$ ratios were normalized against $^{86}Sr/^{88}Sr$ = 0.1194 and $^{146}Nd/^{144}Nd$ = 0.7219
195 respectively, after corrections from isobaric interferences using $^{87}Rb/^{85}Sr$ = 0.387041 on ^{87}Sr
196 and combination of $^{147}Sm/^{149}Sm$ =1.08583 and $^{147}Sm/^{144}Sm$ = 4.87090 on ^{144}Nd.
197
198 **4. Results**
199 **4.1 Petrography**
200 **4.1.1 Host lavas**
201 The host lavas have a microlitic aphyric or porphyritic texture (Fig. 2b-c) with a vacuolar
202 tendency. The groundmass is finely crystallized and made up of dominantly microlites of
203 plagioclase, olivine, pyroxene and opaque minerals microcrystals. The phenocryst phase is
204 dominated by olivine, pyroxene and opaque minerals. The accessory and/or secondary
205 minerals consist of carbonate and chlorite. The clinopyroxene phenocrysts (0.7 – 0.3 mm in
206 size) are elongated and subeuhedral with octagonal basal sections displaying two directions
207 of cleavage (HOL32). Olivine (15.22 – 18.06 wt%) crystals have irregular shapes and various
208 size (0.03 – 0.9 mm) and are often included in pyroxene although some hexagonal basal
209 sections generally cracked, with a core more or less altered or resorbed by the groundmass
210 (Fig. 2c) are locally observed. Some show a fan-shaped radial arrangement. Feldspar
211 phenocrysts (0.02 – 0.4 mm in size) are generally elongated, twinned with intersecting cracks
212 as the twin elongates, and with inclusion of opaque minerals (HOL32). The vacuoles are
213 locally filled with calcium carbonates.

Several samples contain mantle xenoliths or basement enclaves, all exhibiting a reaction rim in contact with the host lava. The crustal enclave displays a medium– to coarse–grained texture, dominated by quartz, potassic feldspars (Kfs) and plagioclase. Fe–Ti oxides and apatite are accessory minerals, while chlorite is secondary.

4.1.2 Mantle xenoliths

Mantle xenoliths and xenocrysts hosted in lavas are rounded or angular fragments of variable size (1 – 8 cm). They are characterized by protogranular or porphyroblastic textures (Fig. 2d-e), and usually display veinlets and melt pockets (Fig. 2g). When the xenocrysts are isolated in the host lavas, they show coronitic reactions consisting either in a spinel overgrowth or a spongy texture. They are essentially made up of four mineral phases including olivine, clinopyroxene, orthopyroxene, and Cr-spinel which are apparently in textural equilibrium. These rock–forming minerals display three generation of crystals: 1) euhedral porphyroblasts locally displaying abundant kink bands, undulose extinction and mechanical twins of orthopyroxene (Fig. 2d), olivine, and Cr-spinel; 2) equidimensional granular neoblasts (Fig. 2f), and 3) microcrystals developed at the expense of porphyroblasts or in intraxenolith melt pools (Fig. 2e-2g). Olivine (41.3 – 69.5 vol.%) occurs as anhedral crystals with angular or sub–rounded shape of variable size (0.5 – 1.5 mm) and often included in pyroxenes. They are generally cracked, often rimmed or partially altered into serpentine (Fig. 2g) or Cr–spinel and locally exhibit undulose extinction. Clinopyroxene (11.2 – 22.2 vol.%) occurs both as small and as large porphyroblasts, often twinned and locally exhibiting undulose extinction. Orthopyroxenes (9.8 – 37.4 vol.%) crystals are midway between olivine and clinopyroxene in term of size (0.2 – 0.7 mm). Both clinopyroxene and orthopyroxene crystals are frequently crosscut by parallel melt veinlets and often display abundant fluid inclusions. Cr–spinels (~ 2 vol.%) are ubiquitous, and occur either as large brown anhedral crystals (0.8 – 1.6 mm) rimmed by thick dark rim more or less altered, or as fine dark microcrystals (< 0.8 mm). The small crystals are dark and mostly present at

241 interstitial position between olivine and pyroxene crystals, or include pyroxene and olivine
242 phenocrysts (Fig. 2d). They are locally surrounded by melt pockets (Fig. 2g).

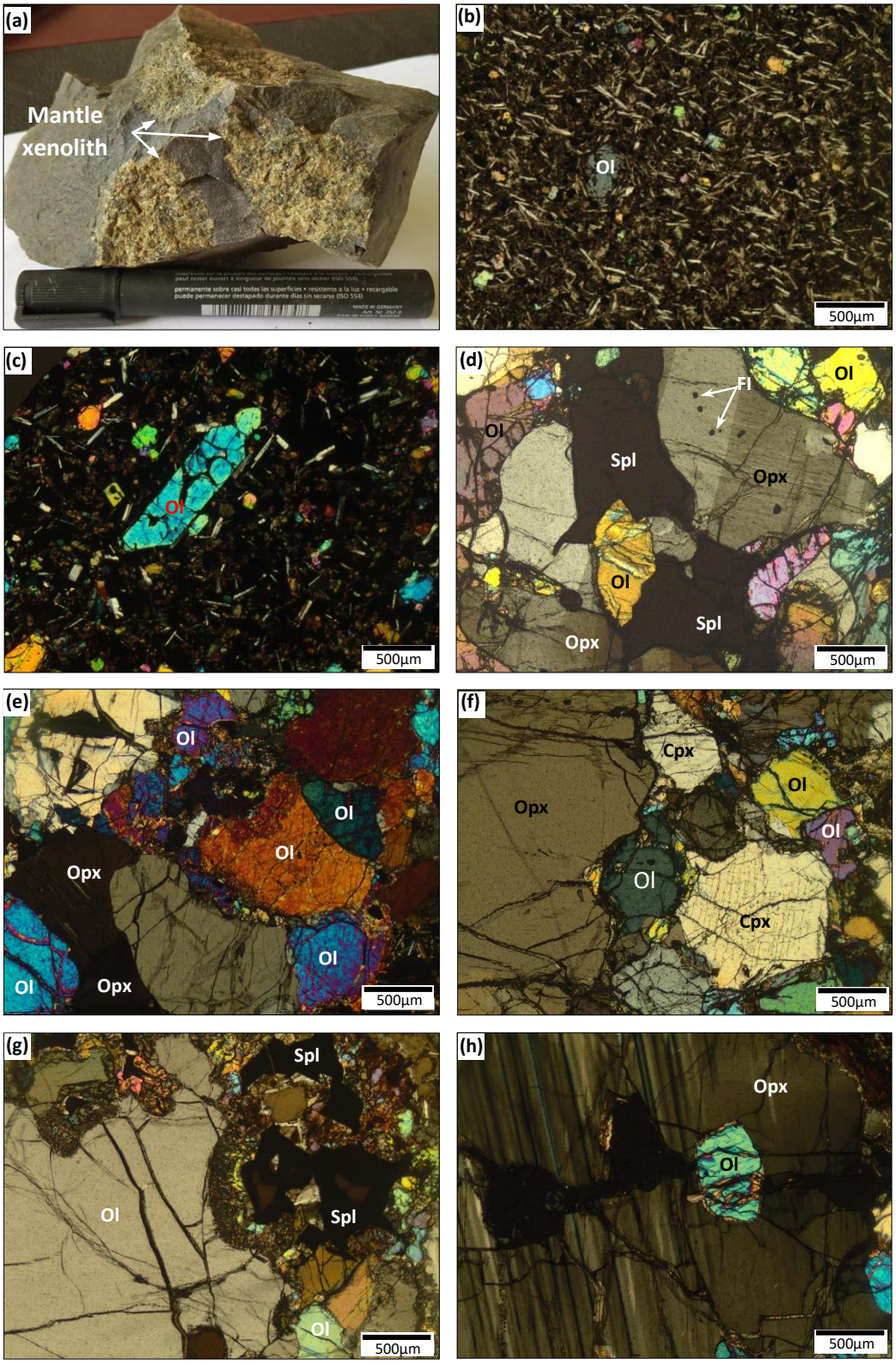

243

Figure 2: Macroscopic view of host lava and photomicrographs taken under crossed-polarized light. (a) lava sample hosting mantle xenoliths; (b) Microlitic aphyric (SAF88) and (c) microlitic porphyritic texture of the study lavas (SOT22); (d) Protogranular texture in a spinel lherzolite with a Cpx crystal showing spinel exsolution lamellae (BIW805); (e) Porphyroblastic texture in spinel lherzolite (BIW88); (f) Melt veinlets crosscutting olivine, Opx and Cpx and twined clinopyroxene crystal displaying numerous fluids inclusions and Cr-spinel encompassing olivine crystal (BIW88); (g) Cumulus olivine crystal altered into serpentine, and melt pocket around spinel crystal (BIW88); (h) Partially altered Opx phenocrystal including olivine and displaying parallel melt veinlets (BIW88). Mineral symbols are from Kretz et al. (1983); FI= fluid inclusion.

4.2 Minerals major elements composition

Some representative microprobe analyses of minerals major element compositions of lavas and hosted lherzolites are presented in Tables 1-4.

4.2.1 Feldspars

Representative feldspars analyses from Bini Warack lavas exhibit wide ranges of CaO (0.1 – 13.8 wt%), Al_2O_3 (18.6 – 30.5 wt%), and FeO (0.1 – 1.12wt%) contents (see Table 1). In the An–Ab–Or ternary diagram (Fig. 3a), plagioclase compositions range from labradorite ($An_{67.43–51.86}$) to albite ($An_{6.64}$) in basanites, from labradorite ($An_{53.21–50.47}$) to andesine ($An_{30.04–30.36}$) in latite. The rare analyzed alkali feldspar is a sanidine ($Ab_{47.55}Or_{52.05}$) xenocryst, also observed in basanite (Sample MBA11 - Analyse C3). A compositional variation marked by a significant enrichment in Al_2O_3, K_2O and CaO and depletion Na_2O from the core to the rim of crystals, is noticed in some andesine crystals of the latite (BJM59A).

4.2.2 Olivine

Olivine crystals from lavas ($Fo_{70.9–90.4}$) display higher FeO (8.7 – 25.7 wt%), CaO (0 – 0.4 wt%) and MnO (0.1 – 0.6 wt%), but lower MgO (35.8 – 49.6 wt%) and NiO (0.1 –0.5 wt%)

contents than those in hosted spinel lherzolites (FeO: 9.5 – 10.2 wt%; MnO: 0.1 – 0.2 wt%; CaO: 0 – 0.1 wt%; NiO: 0.3 – 0.4 wt%; MgO: 47.4 – 49.1 wt%) which are slightly more forsteristic ($Fo_{89.2–91}$ against $Fo_{71–91}$) with lower Fo deviation (~2 mol%) (Table 2). Compositions of olivine xenocrysts present in basanite samples BIW88 and BIW88A (FeO: 8.7 – 14.6 wt%; CaO: 0 – 0.2 wt%; MnO: 0.1 – 0.3 wt%; MgO: 44.7 – 49.2 wt%; NiO: 0.2 – 0.5 wt%) are somewhat comparable with those in lherzolites although one crystal displays lower forsterite content ($Fo_{84.2}$). The Fo contents of Bini Warack lherzolitic olivines fit with the compositional of SCLM olivines (Arai, 1994). Referring to their CaO contents range, olivine grains from lavas are mostly of magmatic origin (CaO > 0.1 wt%) contrary to those in hosted spinel-bearing lherzolites which are of residual origin (mostly CaO < 0.1 wt%) according to Thompson & Gibson (2000). Overall, olivine of spinel lherzolites from Bini Warack displays similar compositions to those of mantle xenoliths from the northern Kapsiki (Tamen et al., 2015) and are more variable compared to those of Nyos (Temdjim et al., 2004), Mount Cameroon (Suh et al., 2008), Kumba (Lee et al., 1996; Teitchou et al., 2007) and Sao Tomé (Caldeira & Munha, 2002). The presence of well-preserved zoned olivine within the studied basaltic lavas is indicative both of a rapid ascent to the surface of their magma, and also of a short duration of the interaction between basaltic melt and hosted lherzolite.

4.2.3 Orthopyroxene

Orthopyroxenes are essentially present in lherzolites, although some xenocrysts are found in some basanites and basalts. The main orthopyroxenes end-members components are $En_{87.6-88.3}Fs_{9-10.5}$ for xenocrysts and $En_{86.8–89.5}Fs_{9–10}$ in lherzolites. There are chemically characterized by CaO (0.3 – 1.3 wt%), Al_2O_3 (2.5 – 5.1 wt%) and exhibit relatively low TiO_2 (0 – 0.2 wt%) and Cr_2O_3 (0.2 – 0.8 wt%) contents. Their Mg# = [100Mg/(Mg + Fe^{2+})] vary between 89.7 and 90.9 and enstatite contents range from 86.8 to 89.5 mol% (Table 3). The studied orthopyroxenes display higher enstatite contents and thus X_{Mg} compared to those from Kapsiki mantle xenoliths (En: 77 – 85 mol%; XMg: 0.89 – 0.92; Tamen et al., 2015).

4.2.4 Clinopyroxene

Clinopyroxene mainly consists of Cr-diopside ($Wo_{46–47}En_{42.6–44}Fs_{4–4.2}Ac_{6–7}$) in lherzolite sometimes associated with pigeonite ($Wo_{11}En_{79}Fs_{8}Ac_{2}$), diopside in basanites and basalts ($Wo_{47–50}En_{27–39}Fs_{11–22}Ac_{2–4}$), and accessory augite ($Wo_{39.8}En_{40.2}Fs_{18}Ac_{2}$) in latite. Their compositions are homogeneous at a sample scale but vary from lherzolites to the host lavas. Cr-diopside is characterized by high X_{Mg} (~ 0.92) and display significant Cr_2O_3 (0.7 – 0.8 wt%), low TiO_2 (0.3 – 0.4 wt%) and constant Al_2O_3 (5.5 – 6.1 wt%) contents compared to diopside found in basanites and basalts which has very low X_{Mg} (0.6 – 0.8), low Cr_2O_3 (0 – 0.4 wt%), and high TiO_2 (2.5 – 7.7 wt%) and Al_2O_3 (5.5 – 11.9 wt%) contents. The single analyzed pigeonite crystal (X_{Mg} = 0.90) found included in a Cr-diopside is Mn-poor (MnO: 0.11 wt%), more aluminous (Al_2O_3: 4.96 wt%) and more magnesian (MgO: 28.4 wt%) relative to those analyzed in peralkaline trachyte from the neighboring Tchabal Mbabo massif (MnO: 3.3 – 3.6 wt%; Bardintzeff et al., 2020) and to those described in trachyandesites from French Massif Central (Maury & Brousse, 1978: MnO= 0.7 – 2 wt%).

Clinopyroxenes within mantle xenoliths of sample BIW805 are characterized by SiO_2 contents ranging between 52.8 and 53.1 wt%, TiO_2 (0.28 – 0.3 wt%), Al_2O_3 (5.5 – 6.2 wt%), CaO (21 – 21.7 wt%), Na_2O (1.65 – 1.7 wt%) and Mg# (92.9 – 94.5), high Al^{VI} and low Al^{IV}/Al^{VI} ratio, similar to clinopyroxenes formed by basaltic melt-mantle peridotite reactions at mantle depths (Yuan & Yan, 2022). The spinel lherzolites from Bini Warack contain olivine with average Mg# of 90, coexisting with Opx of Mg# 90 and Cpx with Mg# 93, which is typical of equilibrium lherzolite assemblages.

Table 1: Representative analyses of feldspars from Bini Warack lavas: (b) =border, (m) = middle and (c) =core

Rock type	Basanite														
Sample	BIW88A			MBA11	SAF88			Sot22							
Analyse	C1	C1 (c)	C4	C3	C1(m)	C3(m)	C4(m)	C1(m)	C3	C3	C4	C4	C5	C5	C5
SiO_2	52.39	53.51	52.32	66.89	52.88	53.54	53.55	51.52	52.91	54.91	52.60	52.10	51.44	51.23	50.53
TiO_2	0.56	0.20	0.15	0.00	0.12	0.16	0.32	0.08	0.15	0.21	0.17	0.16	0.04	0.09	0.12
Al_2O_3	28.49	28.72	29.81	18.56	28.65	29.02	27.43	29.81	28.50	26.25	29.08	28.94	29.40	29.29	29.71
FeO	1.12	0.71	0.47	0.05	0.56	0.63	0.77	0.73	0.44	0.70	0.64	0.64	0.68	0.58	0.68
CaO	11.52	11.28	12.95	0.08	11.56	11.93	11.07	12.80	11.98	8.72	12.34	12.32	13.02	13.16	13.40
Na_2O	4.60	4.75	4.14	5.32	4.75	4.85	5.08	3.74	4.36	5.63	3.88	4.11	3.92	3.83	3.30
K_2O	1.21	0.44	0.33	8.85	0.26	0.29	0.91	0.33	0.47	1.34	0.64	0.58	0.52	0.43	0.42
BaO	-	0.07	-	0.00	0.03	-	-	0.10	0.10	0.61	0.11	0.15	0.01	0.08	0.04
MnO	0.02	0.00	0.01	0.00	0.00	0.03	0.04	0.06	0.03	0.01	0.00	0.01	0.02	0.03	0.09
MgO	0.32	0.03	0.08	0.00	0.08	0.02	0.31	0.09	0.06	0.01	0.04	0.10	0.09	0.05	0.16
NiO	0.02	0.05	0.07	0.00	0.01	0.00	0.00	0.00	0.00	0.00	0.00	0.04	0.00	0.00	0.03
F	-	0.03	-	0.24	0.16	-	-	0.00	0.05	0.00	0.00	0.00	0.37	0.05	0.11
Total	**100.27**	**99.80**	**100.35**	**99.99**	**99.07**	**100.47**	**99.48**	**99.27**	**99.07**	**98.43**	**99.49**	**99.16**	**99.53**	**98.83**	**98.60**
Si	9.61	9.75	9.51	12.059	9.71	9.69	9.84	9.47	9.72	10.16	9.63	9.60	9.48	9.48	9.39
Ti	0.08	0.03	0.02	0.00	0.02	0.02	0.04	0.01	0.02	0.03	0.02	0.02	0.01	0.01	0.02
Al	6.18	6.17	6.39	3.94	6.20	6.19	5.94	6.46	6.17	5.72	6.27	6.28	6.39	6.39	6.51
Fe^{2+}	0.17	0.11	0.07	0.01	0.09	0.10	0.12	0.11	0.07	0.11	0.10	0.10	0.11	0.09	0.11
Ca	2.26	2.20	2.52	0.02	2.28	2.31	2.18	2.52	2.36	1.73	2.42	2.43	2.57	2.61	2.67
Na	1.64	1.68	1.46	1.86	1.69	1.70	1.81	1.33	1.55	2.02	1.38	1.47	1.40	1.37	1.19
K	0.28	0.10	0.08	2.04	0.06	0.07	0.21	0.08	0.11	0.32	0.15	0.14	0.12	0.10	0.10
Ba	0.00	0.01	0.01	0.00	0.00	0.00	0.00	0.01	0.01	0.04	0.01	0.01	0.00	0.01	0.00
SUM	**20.20**	**20.03**	**20.05**	**19.92**	**20.05**	**20.08**	**20.15**	**19.99**	**20.01**	**20.12**	**19.98**	**20.04**	**20.08**	**20.06**	**19.98**
An	54.12	55.30	62.16	0.40	56.49	56.67	51.86	64.13	58.64	42.53	61.32	60.25	62.80	63.88	67.43
Ab	39.11	42.14	35.96	47.55	42.00	41.69	43.07	33.91	38.62	49.69	34.89	36.37	34.22	33.64	30.05
Or	6.77	2.57	1.87	52.05	1.51	1.64	5.08	1.97	2.74	7.78	3.79	3.38	2.97	2.49	2.52

Table 1 (end)

Rock type	Basanite					Latite						
Sample	SOT22				HOL32	BJM59A						
Analyse	C6	C6	C6	C6	C6	C1(m)	C3(c)	C3(c)	C3(b)	C4-(m)	(C5)	C5(m)
SiO_2	52.87	52.70	52.29	51.08	51.50	56.81	61.01	60.46	56.38	55.86	54.70	55.19
TiO_2	0.39	0.16	0.16	0.14	0.10	0.06	0.00	0.00	0.08	0.05	0.07	0.12
Al_2O_3	24.17	29.46	29.04	30.21	30.50	26.39	24.22	24.09	26.26	27.08	27.92	27.51
FeO	1.11	0.62	0.61	0.60	0.50	0.58	0.21	0.20	0.52	0.54	0.45	0.59
CaO	8.72	12.52	12.68	13.86	13.87	9.34	6.42	6.53	9.16	9.92	11.05	10.55
Na_2O	5.56	4.19	4.01	3.41	3.68	5.97	7.89	7.88	6.03	5.49	5.00	5.24
K_2O	2.56	0.32	0.36	0.34	0.33	0.90	0.56	0.60	0.74	0.63	0.56	0.73
BaO	0.31	0.02	0.04	0.04	-	-	-	0.01	0.00	-	-	-
MnO	0.00	0.03	0.04	0.00	0.03	0.00	0.02	0.01	0.04	0.01	0.00	0.00
MgO	0.12	0.06	0.08	0.22	0.09	0.06	0.00	0.01	0.09	0.05	0.12	0.05
NiO	0.00	0.00	0.00	0.00	0.00	0.02	0.00	0.05	0.05	0.00	0.00	0.00
F	0.05	0.00	0.00	0.19	-	-	-	0.08	0.08	-	-	-
Total	**95.96**	**100.08**	**99.31**	**100.09**	**100.63**	**100.14**	**100.33**	**99.92**	**99.42**	**99.63**	**99.87**	**99.98**
Si	10.16	9.57	9.595	9.36	9.36	10.26	10.85	10.83	10.26	10.13	9.93	10.00
Ti	0.06	0.02	0.022	0.02	0.01	0.01	0.00	0.00	0.01	0.01	0.01	0.02
Al	5.48	6.32	6.280	6.52	6.53	5.62	5.08	5.08	5.63	5.79	5.97	5.88
Fe^{2+}	0.18	0.09	0.094	0.09	0.08	0.09	0.03	0.03	0.08	0.08	0.07	0.09
Ca	1.80	2.44	2.493	2.72	2.70	1.81	1.22	1.25	1.79	1.93	2.15	2.05
Na	2.07	1.48	1.427	1.21	1.30	2.09	2.72	2.74	2.13	1.93	1.76	1.84
K	0.63	0.07	0.084	0.08	0.08	0.21	0.13	0.14	0.17	0.15	0.13	0.17
Ba	0.02	0.00	0.00	0.00	0.00	0.00	0.00	0.00	0.00	0.00	0.00	0.00
SUM	**20.39**	**20.01**	**20.00**	**20.01**	**20.05**	**20.07**	**20.03**	**20.07**	**20.06**	**20.01**	**20.02**	**20.05**
An	39.95	61.12	62.26	67.82	66.29	44.03	30.05	30.37	43.72	48.14	53.22	50.46
Ab	46.09	37.02	35.63	30.20	31.83	50.92	66.83	66.31	52.08	48.22	43.57	45.37
Or	13.96	1.86	2.10	1.98	1.88	5.05	3.12	3.32	4.21	3.64	3.21	4.16

Table 2: representative analyses of olivines form study area; (b) =border and (c) =core

Rock type	Basanite																					
Samples	BIW88A									SAF88		Sot22										
Analyses	C1-b	C2 (c)	C2(b)	C2(c)	C3	C3	C4(b)	C4(c)	C4(c)	C1	C3	C2	C2(c)	C2(b)	C1(b)	C1(c)	C3	C4(b)	C4(c)	C5	C6(c)	C6(b)
SiO_2	39.90	39.75	41.28	41.48	41.64	41.75	40.71	41.32	41.35	38.19	39.34	40.16	40.55	39.70	39.84	39.35	40.20	40.26	40.39	38.58	38.97	40.17
TiO_2	0.00	0.10	0.00	0.00	0.00	0.00	0.00	0.00	0.00	0.08	0.00	0.01	0.00	0.00	0.00	0.00	0.00	0.00	0.00	0.00	0.00	0.00
Al_2O_3	0.00	0.10	0.00	0.07	0.00	0.06	0.05	0.00	0.06	0.08	0.02	0.02	0.05	0.03	0.04	0.04	0.06	0.02	0.04	0.08	0.00	0.00
Cr_2O_3	0.00	0.02	0.01	0.04	0.03	0.06	0.01	0.03	0.03	0.01	0.01	0.02	0.04	0.02	0.02	0.00	0.03	0.02	0.03	0.00	0.01	0.03
FeO	18.34	17.61	9.15	8.68	8.83	8.90	10.34	10.08	9.69	25.71	20.04	15.52	14.10	16.42	17.13	19.54	15.03	14.52	15.75	21.91	20.83	14.24
MnO	0.35	0.21	0.18	0.19	0.15	0.16	0.06	0.16	0.05	0.57	0.48	0.27	0.25	0.28	0.21	0.29	0.25	0.22	0.09	0.29	0.23	0.20
MgO	41.49	42.21	48.94	49.34	49.09	49.48	48.02	48.85	48.34	35.83	40.51	43.17	44.77	42.27	42.42	40.37	43.93	44.45	43.54	38.34	39.93	45.05
NiO	0.14	0.10	0.45	0.30	0.44	0.47	0.30	0.45	0.34	0.05	0.21	0.17	0.21	0.17	0.25	0.23	0.24	0.23	0.20	0.05	0.06	0.14
CaO	0.31	0.09	0.12	0.13	0.06	0.08	0.10	0.10	0.12	0.38	0.07	0.36	0.28	0.32	0.11	0.04	0.23	0.27	0.17	0.23	0.14	0.20
Na_2O	0.06	0.00	0.00	0.00	0.00	0.00	0.07	0.03	0.00	0.02	0.00	0.01	0.00	0.00	0.01	0.00	0.02	0.02	0.00	0.03	0.05	0.00
K_2O	0.00	0.00	0.06	0.00	0.06	0.00	0.02	0.03	0.00	0.00	0.00	0.00	0.01	0.00	0.01	0.02	0.00	0.01	0.00	0.03	0.02	0.00
Total	**100.60**	**100.18**	**100.25**	**100.36**	**100.33**	**100.98**	**99.79**	**101.12**	**100.00**	**100.92**	**100.69**	**99.71**	**100.25**	**99.22**	**100.04**	**99.89**	**100.00**	**100.10**	**100.34**	**99.55**	**100.29**	**100.13**
Si	1.01	1.01	1.01	1.01	1.01	1.01	1.00	1.01	1.01	1.00	1.01	1.02	1.01	1.01	1.01	1.01	1.01	1.01	1.01	1.01	1.00	1.01
Ti	0.00	0.00	0.00	0.00	0.00	0.00	0.00	0.00	0.00	0.00	0.00	0.00	0.00	0.00	0.00	0.00	0.00	0.00	0.00	0.00	0.00	0.00
Al	0.00	0.00	0.00	0.00	0.00	0.00	0.00	0.00	0.00	0.00	0.00	0.00	0.00	0.00	0.00	0.00	0.00	0.00	0.00	0.00	0.00	0.00
Cr	0.00	0.00	0.00	0.00	0.00	0.00	0.00	0.00	0.00	0.00	0.00	0.00	0.00	0.00	0.00	0.00	0.00	0.00	0.00	0.00	0.00	0.00
Fe2+	0.39	0.37	0.19	0.18	0.18	0.18	0.21	0.21	0.20	0.57	0.43	0.33	0.29	0.35	0.36	0.42	0.32	0.30	0.33	0.48	0.45	0.30
Mn	0.01	0.00	0.00	0.00	0.00	0.00	0.00	0.00	0.00	0.01	0.01	0.01	0.01	0.01	0.00	0.01	0.01	0.00	0.00	0.01	0.01	0.00
Mg	1.57	1.60	1.78	1.79	1.78	1.78	1.77	1.77	1.76	1.40	1.54	1.63	1.67	1.61	1.60	1.55	1.65	1.66	1.63	1.49	1.53	1.68
Ni	0.00	0.00	0.01	0.01	0.01	0.01	0.01	0.01	0.01	0.00	0.00	0.00	0.00	0.00	0.01	0.00	0.00	0.00	0.00	0.00	0.00	0.00
Ca	0.01	0.00	0.00	0.00	0.00	0.00	0.00	0.00	0.00	0.01	0.00	0.01	0.01	0.01	0.00	0.00	0.01	0.01	0.00	0.01	0.00	0.01
Total	**2.99**	**2.99**	**2.99**	**2.99**	**2.99**	**2.99**	**3.00**	**3.00**	**2.99**	**3.00**	**3.00**	**2.99**	**2.99**	**2.99**	**2.99**	**2.99**	**2.99**	**3.00**	**2.99**	**3.00**	**3.00**	**3.00**
Fo	79.83	80.85	90.34	90.84	90.69	90.68	89.17	89.48	89.85	70.85	77.87	82.97	84.76	81.86	81.35	78.40	83.67	84.31	83.05	75.48	77.17	84.76
Fa	19.79	18.92	9.47	8.96	9.15	9.15	10.77	10.36	10.10	28.51	21.61	16.73	14.97	17.84	18.42	21.28	16.06	15.45	16.85	24.19	22.58	15.03
Tp	0.38	0.23	0.19	0.20	0.16	0.17	0.06	0.17	0.05	0.64	0.52	0.29	0.27	0.31	0.23	0.32	0.27	0.24	0.10	0.32	0.25	0.21

Table 2 (continue)

Rock type	Basanite									Basalt								
Sample					HOL32									MBA11				
Analyse	C1	C2	C2	C4	C4	C4	C5	C5	C5	C1	C2	C2(c)	C2(b)	C2(c)	C4(b)	C4(c)	C5	C5
SiO_2	39.68	40.06	40.53	39.72	40.21	39.76	39.73	39.92	39.90	41.52	40.86	40.95	41.33	41.44	41.53	41.03	42.05	41.55
TiO_2	0.00	0.00	0.01	0.00	0.02	0.00	0.00	0.01	0.00	0.00	0.00	0.00	0.00	0.00	0.00	0.08	0.00	0.00
Al_2O_3	0.00	0.06	0.04	0.07	0.00	0.11	0.00	0.09	0.05	0.07	0.03	0.05	0.08	0.02	0.06	0.04	0.05	0.05
Cr_2O_3	0.00	0.01	0.00	0.05	0.05	0.02	0.01	0.00	0.04	0.02	0.02	0.00	0.03	0.02	0.02	0.00	0.01	0.01
FeO	16.55	16.76	14.5	12.71	12.96	15.09	13.03	15.31	13.77	10.38	11.31	11.68	10.72	10.28	9.47	9.49	8.72	8.94
MnO	0.18	0.09	0.24	0.17	0.22	0.32	0.20	0.27	0.16	0.13	0.21	0.14	0.14	0.11	0.20	0.10	0.12	0.17
MgO	44.02	43.77	45.04	47.55	46.8	45.36	46.69	44.15	45.98	48.35	47.85	47.6	48.21	48.73	48.88	48.47	48.84	49.62
NiO	0.28	0.22	0.25	0.22	0.36	0.28	0.23	0.15	0.32	0.39	0.28	0.42	0.34	0.37	0.5	0.41	0.3	0.36
CaO	0.10	0.15	0.04	0.31	0.22	0.20	0.15	0.05	0.20	0.06	0.05	0.04	0.14	0.11	0.05	0.02	0.04	0.08
Na_2O	0.00	0.01	0.00	0.04	0.01	0.00	0.07	0.05	0.02	0.00	0.02	0.07	0.03	0.02	0.01	0.00	0.11	0.00
K_2O	0.02	0.00	0.00	0.00	0.01	0.03	0.00	0.04	0.00	0.00	0.02	0.01	0.01	0.00	0.03	0.01	0.01	0.00
Total	**100.84**	**101.12**	**100.65**	**100.84**	**100.86**	**101.18**	**100.12**	**100.03**	**100.44**	**100.93**	**100.65**	**100.97**	**101.02**	**101.10**	**100.76**	**99.66**	**100.33**	**100.86**
Si	1.00	1.00	1.01	0.98	1.00	0.99	0.99	1.00	1.00	1.01	1.00	1.00	1.01	1.01	1.01	1.01	1.02	1.01
Ti	0.00	0.00	0.00	0.00	0.00	0.00	0.00	0.00	0.00	0.00	0.00	0.00	0.00	0.00	0.00	0.00	0.00	0.00
Al	0.00	0.00	0.00	0.00	0.00	0.00	0.00	0.00	0.00	0.00	0.00	0.00	0.00	0.00	0.00	0.00	0.00	0.00
Cr	0.00	0.00	0.00	0.00	0.00	0.00	0.00	0.00	0.00	0.00	0.00	0.00	0.00	0.00	0.00	0.00	0.00	0.00
Fe^{2+}	0.35	0.35	0.30	0.26	0.27	0.31	0.27	0.32	0.29	0.21	0.23	0.24	0.22	0.21	0.19	0.19	0.18	0.18
Mn	0.00	0.00	0.01	0.00	0.00	0.01	0.00	0.01	0.00	0.00	0.00	0.00	0.00	0.00	0.00	0.00	0.00	0.00
Mg	1.65	1.63	1.67	1.76	1.73	1.69	1.74	1.66	1.71	1.75	1.75	1.74	1.75	1.77	1.77	1.77	1.77	1.79
Ni	0.01	0.00	0.01	0.00	0.01	0.01	0.00	0.00	0.01	0.01	0.01	0.01	0.01	0.01	0.01	0.01	0.01	0.01
Ca	0.00	0.00	0.00	0.01	0.01	0.01	0.00	0.00	0.01	0.00	0.00	0.00	0.00	0.00	0.00	0.00	0.00	0.00
Total	**3.01**	**3.00**	**2.99**	**3.02**	**3.01**	**3.01**	**3.01**	**3.00**	**3.01**	**2.99**	**3.00**	**3.00**	**2.99**	**3.00**	**2.99**	**2.99**	**2.98**	**2.99**
Fo	82.43	82.24	84.49	86.81	86.36	83.99	86.28	83.47	85.47	89.13	88.10	87.77	88.78	89.32	90.01	90.01	90.78	90.66
Fa	17.38	17.66	15.26	13.01	13.41	15.67	13.51	16.24	14.36	10.73	11.68	12.08	11.07	10.57	9.78	9.88	9.09	9.16
Tp	0.19	0.10	0.26	0.18	0.23	0.34	0.21	0.29	0.17	0.14	0.22	0.15	0.15	0.11	0.21	0.11	0.13	0.18

Table 2 (end)

Rock type	Lherzolite																Xenocrists					
Sample								BIW805									BIW88A			BIW88		
Analyse	C1(b)	C1(c)	C2	C2(b)	C3	C3	C3(c)	C3	C3(c)	C4	C4(c)	C6	C6	C7(b)	C7(c)	C7	C5	C5(b)	C5	C4	C6	C2
SiO_2	41.08	41.37	41.39	41.49	41.11	41.15	41.32	41.01	41.15	41.35	41.19	41.3	41.69	41.28	41.15	41.24	41.4	40.99	40.79	41.59	41.42	40.41
TiO_2	0.01	0.00	0.00	0.00	0.00	0.00	0.00	0.00	0.00	0.00	0.00	0.00	0.00	0.00	0.00	0.00	0.00	0.01	0.00	0.00	0.00	0.00
Al_2O_3	0.06	0.04	0.01	0.05	0.03	0.00	0.03	0.05	0.03	0.04	0.00	0.01	0.00	0.00	0.05	0.03	0.04	0.02	0.00	0.04	0.05	0.06
Cr_2O_3	0.05	0.00	0.01	0.01	0.01	0.01	0.00	0.00	0.00	0.01	0.00	0.02	0.00	0.01	0.00	0.00	0.03	0.03	0.04	0.00	0.01	0.02
FeO	10.07	9.76	9.69	9.64	9.56	9.62	9.59	9.66	9.62	9.53	9.62	9.67	9.78	9.79	9.72	9.65	8.67	8.96	9.68	10.23	10.01	14.75
MnO	0.13	0.10	0.15	0.19	0.13	0.15	0.13	0.14	0.10	0.10	0.10	0.13	0.11	0.17	0.11	0.14	0.15	0.15	0.18	0.11	0.16	0.25
MgO	47.38	47.98	48.82	48.26	48.52	48.30	48.00	48.27	48.38	48.15	48.27	48.51	49.09	48.62	48.79	48.49	49.17	49.56	48.58	48.58	48.62	44.67
NiO	0.37	0.42	0.30	0.33	0.33	0.39	0.36	0.44	0.32	0.36	0.37	0.35	0.34	0.43	0.34	0.43	0.52	0.40	0.42	0.44	0.38	0.22
CaO	0.12	0.11	0.06	0.04	0.07	0.05	0.04	0.07	0.08	0.06	0.08	0.07	0.03	0.02	0.04	0.06	0.05	0.08	0.09	0.03	0.02	0.19
Na_2O	0.03	0.00	0.00	0.00	0.02	0.00	0.01	0.00	0.00	0.03	0.04	0.00	0.00	0.04	0.00	0.00	0.00	0.01	0.00	0.00	0.00	0.04
K_2O	0.00	0.00	0.00	0.02	0.00	0.00	0.00	0.03	0.00	0.01	0.05	0.00	0.00	0.02	0.02	0.00	0.00	0.00	0.03	0.01	0.00	0.00
Total	**99.29**	**99.77**	**100.43**	**100.03**	**99.79**	**99.67**	**99.48**	**99.67**	**99.68**	**99.64**	**99.73**	**100.06**	**101.04**	**100.37**	**100.24**	**100.05**	**100.06**	**100.33**	**99.82**	**101.03**	**100.68**	**100.62**
Si	1.02	1.02	1.01	1.01	1.01	1.01	1.02	1.01	1.01	1.02	1.01	1.01	1.01	1.01	1.01	1.01	1.01	1.00	1.00	1.01	1.01	1.01
Ti	0.00	0.00	0.00	0.00	0.00	0.00	0.00	0.00	0.00	0.00	0.00	0.00	0.00	0.00	0.00	0.00	0.00	0.00	0.00	0.00	0.00	0.00
Al	0.00	0.00	0.00	0.00	0.00	0.00	0.00	0.00	0.00	0.00	0.00	0.00	0.00	0.00	0.00	0.00	0.00	0.00	0.00	0.00	0.00	0.00
Cr	0.00	0.00	0.00	0.00	0.00	0.00	0.00	0.00	0.00	0.00	0.00	0.00	0.00	0.00	0.00	0.00	0.00	0.00	0.00	0.00	0.00	0.00
Fe^{2+}	0.21	0.20	0.20	0.20	0.20	0.20	0.20	0.20	0.20	0.20	0.20	0.20	0.20	0.20	0.20	0.20	0.18	0.18	0.20	0.21	0.20	0.31
Mn	0.00	0.00	0.00	0.00	0.00	0.00	0.00	0.00	0.00	0.00	0.00	0.00	0.00	0.00	0.00	0.00	0.00	0.00	0.00	0.00	0.00	0.01
Mg	1.75	1.76	1.77	1.76	1.78	1.77	1.76	1.77	1.77	1.76	1.77	1.77	1.77	1.77	1.78	1.77	1.79	1.80	1.78	1.76	1.77	1.66
Ni	0.01	0.01	0.01	0.01	0.01	0.01	0.01	0.01	0.01	0.01	0.01	0.01	0.01	0.01	0.01	0.01	0.01	0.01	0.01	0.01	0.01	0.00
Ca	0.00	0.00	0.00	0.00	0.00	0.00	0.00	0.00	0.00	0.00	0.00	0.00	0.00	0.00	0.00	0.00	0.00	0.00	0.00	0.00	0.00	0.01
Total	**2.99**	**2.99**	**2.99**	**2.99**	**2.99**	**2.99**	**2.98**	**2.99**	**2.99**	**2.99**	**2.99**	**2.99**	**2.99**	**2.99**	**2.99**	**2.99**	**2.99**	**3.00**	**3.00**	**2.99**	**2.99**	**3.00**
Fo	89.22	89.66	89.84	89.74	89.93	89.81	89.80	89.78	89.87	89.91	89.85	89.82	89.85	89.69	89.85	89.83	90.86	90.65	89.78	89.33	89.50	84.15
Fa	10.64	10.23	10.00	10.05	9.94	10.03	10.06	10.08	10.02	9.98	10.04	10.04	10.04	10.13	10.04	10.03	8.99	9.19	10.03	10.55	10.33	15.58
Tp	0.14	0.11	0.16	0.20	0.14	0.16	0.14	0.15	0.11	0.11	0.11	0.14	0.11	0.18	0.12	0.15	0.16	0.16	0.19	0.11	0.17	0.27

Table 3: Representative analyses of pyroxenes; a- clinopyroxenes

Rock type	Basanite							Latite	Lherzolite		
Sample	Sot22		HOL32			BIW88		BJM59A	BIW805		
Analyse	C6	C6	C1	C1	C1	C5 (i)	C6	C5	C3	C7(i)	C2(i)
SiO_2	47.25	37.41	46.86	44.64	47.99	53.02	53.14	49.38	53.09	52.82	52.8
TiO_2	3.58	7.67	2.54	3.95	2.47	0.37	0.34	1.65	0.29	0.28	0.30
Al_2O_3	6.69	11.07	5.58	8.20	5.47	6.12	5.90	4.52	5.51	5.92	6.15
Cr_2O_3	0.03	0.00	0.08	0.42	0.12	0.80	0.78	0.13	0.70	0.00	0.00
FeO	8.85	12.02	7.20	7.19	6.89	2.33	2.40	10.73	2.41	2.41	2.44
MnO	0.26	0.23	0.09	0.11	0.21	0.09	0.03	0.22	0.13	0.03	0.14
MgO	10.82	8.25	13.38	11.84	13.63	14.50	14.68	13.69	14.82	14.8	14.86
CaO	21.37	19.86	23.19	22.74	22.86	22.11	22.09	18.82	21.44	21.68	20.98
Na_2O	0.79	0.89	0.44	0.56	0.42	1.73	1.61	0.52	1.66	1.65	1.70
K_2O	0.13	0.19	0.00	0.01	0.00	0.00	0.00	0.00	0.00	0.01	0.01
NiO	0.11	0.00	0.03	0.00	0.05	0.00	0.00	0.00	0.04	0.06	0.03
Total	**99.88**	**97.59**	**99.39**	**99.66**	**100.11**	**101.07**	**100.97**	**99.66**	**100.09**	**99.66**	**99.41**
Si	1.78	1.49	1.77	1.69	1.79	1.90	1.91	1.86	1.92	1.92	1.92
Al^{IV}	0.22	0.51	0.23	0.31	0.21	0.10	0.09	0.14	0.08	0.09	0.08
Al^{VI}	0.08	0.01	0.02	0.05	0.03	0.16	0.16	0.06	0.15	0.17	0.18
Fe^{3+}	0.00	0.18	0.14	0.10	0.09	0.03	0.02	0.04	0.01	0.03	0.01
Cr	0.00	0.00	0.00	0.01	0.00	0.02	0.02	0.00	0.02	0.00	0.00
Ti	0.10	0.23	0.07	0.11	0.07	0.01	0.01	0.05	0.01	0.01	0.01
Fe^{2+}	0.28	0.22	0.08	0.12	0.12	0.04	0.06	0.29	0.06	0.05	0.06
Mn	0.01	0.01	0.00	0.00	0.01	0.00	0.00	0.01	0.00	0.00	0.00
Mg	0.61	0.49	0.75	0.67	0.76	0.76	0.79	0.77	0.80	0.80	0.80
Ca	0.86	0.85	0.94	0.92	0.96	0.85	0.85	0.76	0.83	0.84	0.82
Na	0.06	0.07	0.03	0.04	0.03	0.12	0.11	0.04	0.12	0.12	0.12
K	0.01	0.01	0.00	0.00	0.00	0.00	0.00	0.00	0.00	0.00	0.00
SUM	**4.00**	**4.06**	**4.05**	**4.03**	**4.03**	**4.01**	**4.01**	**4.01**	**4.00**	**4.01**	**4.01**
$Fe^{2+}/(Fe^{2+}+Fe^{3+})$	0.99	0.54	0.37	0.55	0.56	0.62	0.79	0.88	0.84	0.64	0.81
XMg	0.69	0.70	0.90	0.84	0.86	0.95	0.93	0.72	0.93	0.95	0.93
Wo	47.52	46.87	48.08	49.56	47.54	46.740	46.68	39.76	45.57	45.97	44.88
En	33.48	27.09	38.61	35.91	39.44	42.66	43.17	40.25	43.83	43.67	44.23
Fs	15.81	22.24	11.66	12.32	11.44	3.99	4.00	18.00	4.21	4.03	4.31
Ac	3.18	3.80	1.65	2.21	1.58	6.62	6.16	1.99	6.39	6.33	6.58

Table 3b- Orthopyroxenes: (b) =border, (c) =core and (i) =inclusion.

Rock type						Basanite												Lherzolite					
Sample	MBA11	BIW88A						BIW88					BIW805										
Analyses	C1	C3(i)	C3-1	C3(i)	C2	C4 (b)	C4(c)	C4	C5(b)	C5(c)	C6(b)	C6(c)	C1(b)	C1 (c)	C2(c)	C2	C4(c)	C4(c)	C6 (b)	C6 (c)	C6 (c)	C6(i)
SiO_2	55.70	55.96	57.63	57.27	56.17	56.00	56.07	55.61	56.00	55.08	56.12	56.11	56.07	56.10	55.73	55.48	55.91	55.77	56.3	56.46	54.96	55.51
TiO_2	0.10	0.06	0.03	0.05	0.06	0.06	0.06	0.05	0.07	0.17	0.05	0.06	0.05	0.04	0.06	0.06	0.04	0.04	0.05	0.04	0.04	0.06
Al_2O_3	4.71	3.66	2.50	2.59	3.93	4.11	4.15	4.44	3.94	4.96	3.82	4.13	3.38	3.55	4.23	4.18	3.57	3.54	3.04	3.15	5.05	5.05
Cr_2O_3	0.33	0.76	0.15	0.16	0.33	0.37	0.37	0.39	0.35	0.53	0.32	0.36	0.22	0.28	0.37	0.34	0.29	0.27	0.24	0.25	0.42	0.45
FeO	6.65	5.74	6.63	6.50	6.67	6.70	6.63	6.44	6.68	5.64	6.68	6.66	6.26	6.39	6.59	6.40	6.34	6.55	6.26	6.32	6.31	6.31
MnO	0.23	0.14	0.07	0.13	0.16	0.18	0.13	0.16	0.18	0.11	0.13	0.14	0.22	0.15	0.17	0.21	0.14	0.14	0.23	0.10	0.17	0.20
MgO	32.29	32.43	34.39	33.73	32.97	32.95	33.17	33.01	33.28	28.43	33.36	33.19	32.67	32.65	32.98	32.49	32.54	32.79	33.31	33.43	32.04	31.3
CaO	0.73	1.18	0.37	0.30	0.37	0.30	0.33	0.37	0.32	5.44	0.31	0.33	0.47	0.50	0.40	0.51	0.58	0.46	0.29	0.36	0.82	1.26
Na_2O	0.13	0.12	0.04	0.04	0.05	0.06	0.05	0.07	0.05	0.44	0.02	0.02	0.08	0.04	0.04	0.04	0.06	0.04	0.05	0.04	0.12	0.15
K_2O	0.00	0.01	0.00	0.00	0.00	0.00	0.00	0.00	0.00	0.01	0.00	0.00	0.00	0.00	0.00	0.00	0.00	0.00	0.03	0.01	0.02	0.01
NiO	0.14	0.08	0.13	0.11	0.11	0.08	0.09	0.11	0.11	0.08	0.06	0.09	0.07	0.06	0.10	0.08	0.10	0.10	0.11	0.12	0.07	0.04
TOTAL	**101.01**	**100.14**	**101.94**	**100.88**	**100.82**	**100.81**	**101.05**	**100.65**	**100.98**	**100.89**	**100.87**	**101.09**	**99.49**	**99.76**	**100.67**	**99.79**	**99.57**	**99.7**	**99.91**	**100.28**	**100.02**	**100.34**
Si	1.91	1.93	1.95	1.96	1.93	1.92	1.92	1.91	1.92	1.91	1.92	1.92	1.94	1.94	1.91	1.92	1.94	1.93	1.94	1.94	1.90	1.91
Al	0.09	0.07	0.05	0.04	0.08	0.08	0.08	0.09	0.08	0.09	0.08	0.08	0.06	0.06	0.09	0.08	0.06	0.07	0.06	0.06	0.10	0.09
Al	0.10	0.08	0.05	0.06	0.08	0.09	0.08	0.09	0.08	0.11	0.08	0.08	0.08	0.08	0.09	0.09	0.08	0.08	0.07	0.07	0.11	0.12
Fe^{3+}	0.00	0.00	0.00	0.00	0.00	0.00	0.00	0.00	0.00	0.00	0.00	0.00	0.00	0.00	0.00	0.00	0.00	0.00	0.00	0.00	0.00	0.00
Cr	0.01	0.02	0.00	0.00	0.01	0.01	0.01	0.01	0.01	0.02	0.01	0.01	0.01	0.01	0.01	0.01	0.01	0.01	0.01	0.01	0.01	0.01
Ti	0.00	0.00	0.00	0.00	0.00	0.00	0.00	0.00	0.00	0.00	0.00	0.00	0.00	0.00	0.00	0.00	0.00	0.00	0.00	0.00	0.00	0.00
Fe^{2+}	0.19	0.17	0.19	0.19	0.19	0.19	0.19	0.19	0.19	0.16	0.19	0.19	0.18	0.19	0.19	0.19	0.18	0.19	0.18	0.18	0.18	0.18
Mn	0.01	0.00	0.00	0.00	0.01	0.01	0.00	0.01	0.01	0.00	0.00	0.00	0.01	0.00	0.01	0.01	0.00	0.00	0.01	0.00	0.01	0.01
Mg	1.65	1.67	1.74	1.72	1.68	1.68	1.69	1.69	1.70	1.47	1.70	1.69	1.69	1.68	1.69	1.68	1.68	1.69	1.71	1.71	1.65	1.61
Ca	0.03	0.04	0.01	0.01	0.01	0.01	0.01	0.01	0.01	0.20	0.01	0.01	0.02	0.02	0.02	0.02	0.02	0.02	0.01	0.01	0.03	0.05
Na	0.01	0.01	0.00	0.00	0.00	0.00	0.00	0.01	0.00	0.03	0.00	0.00	0.01	0.00	0.00	0.00	0.00	0.00	0.00	0.00	0.01	0.01
K	0.00	0.00	0.00	0.00	0.00	0.00	0.00	0.00	0.00	0.00	0.00	0.00	0.00	0.00	0.00	0.00	0.00	0.00	0.00	0.00	0.00	0.00
SUM	**3.99**	**3.99**	**4.00**	**3.99**	**3.99**	**3.99**	**4.00**	**4.00**	**4.00**	**4.00**	**4.00**	**3.99**	**4.00**	**3.99**	**4.00**	**3.99**	**3.99**	**3.99**	**3.99**	**3.99**	**4.00**	**3.98**
$Fe^{2+}/(Fe^{2+}+Fe^{3+})$	1.00	1.00	1.00	1.00	1.00	1.00	1.00	1.00	1.00	1.00	1.00	1.10	1.00	1.00	1.00	1.00	1.00	1.00	1.00	1.00	1.00	1.00
XMg	0.90	0.91	0.90	0.90	0.90	0.90	0.90	0.90	0.90	0.90	0.90	0.90	0.90	0.90	0.90	0.90	0.90	0.90	0.90	0.90	0.90	0.90
Wo	1.42	2.31	0.69	0.57	0.72	0.58	0.64	0.72	0.61	10.82	0.60	0.64	0.92	0.98	0.77	1.00	1.14	0.90	0.56	0.69	1.62	2.51
En	87.62	88.26	89.40	89.40	88.77	88.79	89.00	89.04	88.92	78.66	89.12	89.04	88.87	88.86	88.86	88.71	88.71	88.78	89.47	89.51	87.96	86.78
Fs	10.49	9.00	9.78	9.89	10.34	10.42	10.19	10.00	10.29	8.94	10.22	10.25	9.92	10.02	10.23	10.15	9.94	10.18	9.80	9.66	9.99	10.17
Ac	0.46	0.43	0.14	0.14	0.18	0.21	0.17	0.25	0.17	1.58	0.07	0.07	0.28	0.14	0.14	0.14	0.21	0.14	0.18	0.14	0.43	0.54

Table 4: Representative analyses of spinels. FeO and Fe_2O_3 have been recalculated from analytic microprobe FeOt; (b)=border, (c)=core and (i) = inclusion

Rock type	Basanite												Latite		Lherzolite								
Sample	Sot22		HOL32	BIW88A				MBA11		SAF88			BJM59A		BIW805							BIW88	
Comment	C5	C6(b)	C6	C1(i)	C3	C5	C4	C5	C1	C1(b)	C1(c)	C3	C4	C5	C2	C2	C4	C4 (c)	C6 (b)	C7	C3	C1	C2
SiO_2	0.00	0.14	0.01	0.09	0.09	0.00	0.07	0.11	0.05	0.02	0.00	0.01	0.04	0.72	0.02	0.00	0.01	0.01	0.04	0.02	0.03	8.52	0.02
TiO_2	20.11	21.05	20.77	22.76	0.00	24.72	24.54	1.85	21.48	21.03	0.05	23.76	4.94	46.88	0.00	0.03	0.01	0.02	0.01	0.00	0.00	3.39	0.07
Al_2O_3	6.73	6.01	7.07	5.95	37.78	4.13	4.10	28.62	2.45	4.46	43.07	2.83	0.72	0.12	55.33	55.39	55.52	55.61	55.87	55.26	56.84	32.38	54.47
Cr_2O_3	0.67	0.50	0.64	1.43	28.56	0.40	0.31	24.73	0.91	1.92	21.67	0.12	0.01	0.04	9.51	9.77	9.45	9.57	9.06	9.43	10.26	13.69	9.57
V_2O_3	0.19	0.17	-	-	0.02	-	-	-	-	-	-	-	-	-	-	-	-	-	-	-	-	-	0.00
FeO	42.86	44.66	40.65	44.63	10.28	47.10	46.83	19.61	44.42	42.71	17.05	46.25	58.02	42.39	8.69	8.79	8.34	8.64	8.54	8.81	9.43	25.73	11.48
Fe_2O_3c	23.63	20.75	22.79	19.31	4.41	18.66	19.08	12.33	25.29	23.47	2.85	22.68	35.01	0.00	4.08	3.65	4.27	3.91	3.94	4.10	2.21	0.00	4.09
MnO	0.63	0.50	0.48	0.63	0.15	0.80	0.76	0.42	0.85	0.70	0.38	0.78	0.57	5.93	0.06	0.08	0.16	0.11	0.09	0.07	0.08	0.32	0.24
MgO	4.74	3.84	6.47	5.29	17.89	4.50	4.63	11.73	3.82	5.03	13.76	4.40	0.00	0.01	20.52	20.46	20.78	20.63	20.68	20.42	20.33	11.56	18.61
CaO	0.00	0.06	0.20	0.01	0.00	0.03	0.06	0.04	0.16	0.08	0.00	0.11	0.01	0.95	0.03	0.00	0.00	0.00	0.03	0.00	0.00	2.30	0.01
ZnO	0.01	0.00	-	-	0.00	-	-	-	-	-	-	-	-	-	-	-	-	-	-	-	-	-	0.01
Na_2O	0.06	0.02	0.06	0.04	0.01	0.02	0.00	0.00	0.00	0.00	0.01	0.07	0.00	0.00	0.00	0.00	0.00	0.00	0.03	0.00	0.00	0.75	0.02
K2O	0.00	0.04	0.03	0.00	0.00	0.02	0.00	0.01	0.05	0.00	0.00	0.02	0.00	0.02	0.02	0.00	0.00	0.00	0.00	0.00	0.00	0.07	0.00
NiO	0.09	0.06	0.14	0.08	0.27	0.06	0.12	0.07	0.12	0.01	0.34	0.04	0.06	0.00	0.36	0.35	0.41	0.37	0.44	0.36	0.34	0.25	0.36
BaO	0.03	0.00	-	-	0.59	-	-	-	-	-	-	-	-	-	-	-	-	-	-	-	-	-	0.09
Total	**99.76**	**97.80**	**99.30**	**100.22**	**100.05**	**100.44**	**100.50**	**99.52**	**99.60**	**99.43**	**99.18**	**101.06**	**99.38**	**97.06**	**98.62**	**98.52**	**98.95**	**98.87**	**98.74**	**98.47**	**99.52**	**98.96**	**99.04**
Si	0.00	0.04	0.00	0.03	0.02	0.00	0.02	0.03	0.01	0.01	0.00	0.00	0.01	0.22	0.00	0.00	0.00	0.00	0.01	0.00	0.01	2.01	0.00
Ti	4.27	4.59	4.37	4.80	0.00	5.27	5.23	0.34	4.70	4.51	0.01	5.08	1.14	10.90	0.00	0.00	0.00	0.00	0.00	0.00	0.00	0.60	0.01
Al	2.24	2.05	2.33	1.97	10.09	1.38	1.37	8.23	0.84	1.50	11.58	0.95	0.26	0.04	13.76	13.78	13.75	13.78	13.85	13.76	13.95	9.02	13.70
Cr	0.15	0.11	0.14	0.32	5.12	0.09	0.07	4.77	0.21	0.43	3.91	0.03	0.00	0.01	1.59	1.63	1.57	1.59	1.51	1.58	1.69	2.56	1.61
V	0.04	0.04	0.00	0.00	0.00	0.00	0.00	0.00	0.00	0.00	0.00	0.00	0.00	0.00	0.00	0.00	0.00	0.00	0.00	0.00	0.00	0.00	0.00
Fe^{3+}	5.02	4.53	4.79	4.07	0.75	3.98	4.07	2.26	5.53	5.04	0.49	4.85	13.43	0.00	0.65	0.58	0.67	0.62	0.62	0.65	0.35	0.00	0.66
Fe^{2+}	10.12	10.83	9.50	10.46	1.95	11.17	11.09	4.00	10.80	10.18	3.25	11.00	9.00	10.96	1.53	1.55	1.47	1.52	1.50	1.56	1.68	5.09	2.05
Mn	0.15	0.12	0.11	0.15	0.03	0.19	0.18	0.09	0.21	0.17	0.07	0.19	0.15	1.55	0.01	0.01	0.03	0.02	0.02	0.01	0.01	0.06	0.04
Mg	2.00	1.66	2.70	2.21	6.04	1.90	1.96	4.27	1.66	2.14	4.68	1.87	0.00	0.00	6.45	6.44	6.51	6.47	6.48	6.43	6.31	4.07	5.92
Ca	0.00	0.02	0.06	0.00	0.00	0.01	0.02	0.01	0.05	0.02	0.00	0.03	0.00	0.31	0.01	0.00	0.00	0.00	0.01	0.00	0.00	0.58	0.00
Zn	0.00	0.00	0.00	0.00	0.00	0.00	0.00	0.00	0.00	0.00	0.00	0.00	0.00	0.00	0.00	0.00	0.00	0.00	0.00	0.00	0.00	0.00	0.00
SUM	**24.00**	**24.00**	**24.00**	**24.00**	**24.00**	**24.00**	**24.00**	**24.00**	**24.00**	**24.00**	**24.00**	**24.00**	**24.00**	**24.00**	**24.00**	**24.00**	**24.00**	**24.00**	**24.00**	**24.00**	**24.00**	**24.00**	**24.00**
Fe/Fe+Mg	0.88	0.90	0.84	0.87	0.31	0.89	0.89	0.59	0.91	0.88	0.44	0.89	1.00	1.00	0.25	0.25	0.25	0.25	0.25	0.26	0.24	0.56	0.31
Cr/Cr+Al	0.06	0.05	0.06	0.14	0.34	0.06	0.05	0.37	0.20	0.22	0.25	0.03	0.01	0.18	0.10	0.11	0.10	0.10	0.10	0.10	0.11	0.22	0.11
Fe^{2+}/Fe^{3+}	2.02	2.39	1.98	2.57	2.59	2.80	2.73	1.77	1.95	2.02	6.66	2.27	0.67	-	2.36	2.68	2.17	2.45	2.41	2.39	4.85	#DIV/0!	3.12
Mg#	9.96	7.92	13.73	10.60	63.50	8.72	9.00	37.43	7.92	10.54	44.66	8.69	0.00	0.02	70.26	69.95	71.35	70.48	70.77	69.85	68.31	31.00	61.86

4.2.5 Spinel

Spinels occuring in host lavas are mainly aluminous magnetites and rarely chromiferous spinels while those in lherzolites are essentially chromiferous spinels. Basanites contain the most ferriferous, titaniferous spinels while the hosted lherzolites have the most aluminous and magnesian spinels (Tab. 4). In comparison to the spinels of lavas [Cr# (Cr/(Al + Cr): 0.01 – 0.37; XFe: 0.31 – 1; Mg# ≤ 45], spinels from hosted lherzolites usually have higher Cr# (0.1 – 0.22), higher Mg# (31 – 71) and lower XFe (0.24 – 0.56) and mainly plot within the fertile peridotite field in the Cr# vs. Mg# diagram (Fig. 3d). The spinels Cr# values of the studied lherzolites are in the same range as those of mantle xenoliths from several localities from the CVL such as Wum (0.02 – 0.29: Puziewicz et al., 2023), Kapsiki (0.13 – 0.44; Tamen et al., 2015) Nyoss (0.1 – 0.39: Temdjim et al., 2004, Teitchou et al., 2011). The wide ranges of Fe^{2+}/Fe^{3+}ratios (0.67 – 6.63) and TiO_2 contents (0 – 46.88 wt%) testify to the presence of both mantle spinels (TiO_2 < 0.2 wt%; Fe^{2+}/Fe^{3+} > 2) and magmatic spinels in host lavas, according to Kamenetsky et al. (2001). Most analyzed spinels from lavas display extremely high TiO_2 contents (~20 – 47 wt%), far above those of xenocrysts or spinels found in other lavas from other localities along the CVL (Nono et al., 1994, Tamen et al., 2007).

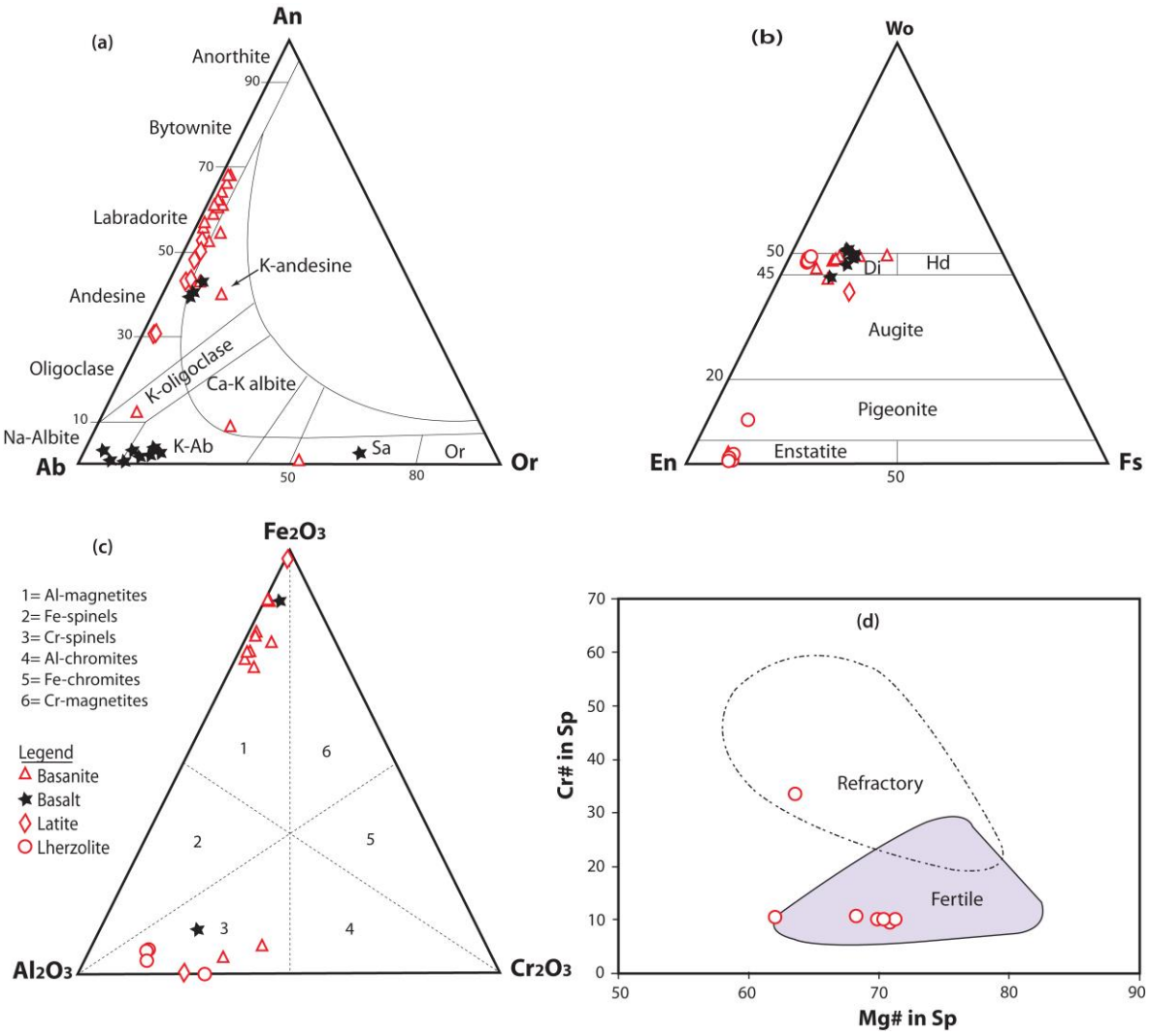

Figure 3: Chemical composition of the main mineral phases of the Bini lavas and hosted spinel lherzolites: a) representative feldspars in the ternary An–Ab–Or diagram of Smith & Brown (1988); b) Analyzed clinopyroxenes in the ternary Wo–En–Fs diagram of Morimoto et al. (1988); c) Ti-Fe oxides in the ternary Fe_2O_3–Al_2O_3–Cr_2O_3 diagram of Stevens (1944); d) Spinels Cr# vs. Mg# diagram, the refractory and fertile peridotite fields are from Bian et al. (2024). Some data of feldspars and pyroxenes from Tiabou et al. (2019) were also used for these diagrams (in black colour). For minerals symbols, Ab=albite, An=anorthite, Sa=Sanidine, Or=orthoclase, En=Enstatite, Di=Diopside, Fs=ferrosilite, Wo=wollastonite, Hd=hedenbergite, Sp=spinel

4.3 Whole rock geochemistry

Major and trace element compositions of 21 representative samples of the host lavas (6 from this study and 15 from Tiabou et al., 2019) and 6 mantle xenoliths are presented in Table 5 and Table 6 respectively. Because of loss on ignition values higher than 2 wt% in most of the analyzed samples, the results were recomputed on an anhydrous base.

4.3.1 Host lavas

Major elements

Although few samples diplay Na_2O-K_2O>2 majority of the studied samples are sodic, therefore we have chosen the TAS classification diagram instead of the potassic series one. The analyzed host lavas plot in the field of basanite, basalt and basaltic trachyandesite on the classification diagram of LeBas et al., 1986 (Fig. 4a). Since the sample BJM59A ploting in the field of basaltic trachyandesite has (Na_2O-2) < K_2O, it will be considered rather as a latite. SiO_2 ranges from 42.35 to 56.56 wt%, the total alkali (Na_2O+K_2O) varies from 2.34 to 7.07 wt% and Na_2O/K_2O ratios from 0.94 to 1.92 with moderate MgO contents (3.56 – 13.86 wt%), and Mg# (43.07 – 70.56). Their differentiation index (DI) ranges from 21.3 (basanite HOL32) to 53.6 (latite) with Mg numbers varying between 43 and 71.

All the analyzed samples are apatite (1.12 – 3.52 wt%) and ilmenite (3.12 to 7.31 wt%) normative, and the silica-undersaturated lavas (basanites and basalts) are nepheline (4.31 – 18.21 wt%) normative. The only lava without normative nepheline nor olivine but containing normative quartz (4.82 wt%) and hypersthene (16.14 wt%) is the sample BJM59A, classified as a latite. Mafic lavas are alkaline sodic (Na_2O/K_2O: 1.14 – 1.92) while latite is potassic with Na_2O/K_2O = 0.94.

In the Harker diagrams (Fig. 5), Al_2O_3 shows a positive correlation with SiO_2 while Fe_2O_{3T}, CaO, P_2O_5, and TiO_2 are negatively correlated with SiO_2. The positive correlation of Al_2O_3 with SiO_2 is indicative of non-fractionation of plagioclase while the negative trends in Fe_2O_{3T}, CaO, TiO_2 and P_2O_5 versus SiO_2 reveal the fractionation of olivine, pyroxenes, Fe–Ti oxides and apatite, respectively.

Table 5: Whole rock chemical analyses of 21 representative host lavas: 6 from this study (Italic bold) and 15 from Tiabou et al. (2019)

Rock type	Basanite										
Sample	**BIW 88A**	**HOL 32**	**SAF 88**	**SOT 22**	**MBA 11**	**PK8**	**PK3**	**BA19**	**BA20**	**BA50**	**BA5**
SiO_2	***40.84***	***41.5***	***41.86***	***42.38***	***43.47***	42.79	42.84	39.2	41.99	41.68	42.68
TiO_2	***3.50***	***2.87***	***3.70***	***2.82***	***2.49***	2.99	3.01	3.01	3.16	3.16	3.16
Al_2O_3	***12.59***	***11.98***	***13.94***	***12.4***	***12.6***	13.88	13.29	11.49	12.89	12.87	12.82
Fe_2O_3	***13.18***	***12.42***	***13.96***	***12.61***	***11.05***	12.06	11.99	13.9	14.32	13.99	14.22
MnO	***0.19***	***0.19***	***0.22***	***0.19***	***0.16***	0.20	0.19	0.22	0.28	0.24	0.19
MgO	***10.62***	***11.35***	***7.47***	***11.36***	***13.37***	7.69	7.63	8.14	7.15	7.16	7.21
CaO	***10.67***	***11.22***	***9.44***	***10.71***	***8.33***	9.88	9.89	12.31	9.33	9.31	8.93
Na_2O	***2.57***	***1.83***	***3.35***	***2.58***	***2.74***	3.30	3.29	3.99	4.35	4.47	4.29
K_2O	***1.38***	***1.60***	***1.98***	***1.72***	***1.53***	1.29	1.33	2.03	2.27	2.37	2.27
P_2O_5	***0.92***	***0.92***	***1.46***	***0.92***	***0.71***	1.16	1.20	1.39	1.44	1.44	1.43
TOTAL (wt.%)	***96.46***	***95.88***	***97.38***	***97.69***	***96.45***	**95.24**	**94.66**	**95.68**	**97.18**	**96.69**	**97.20**
LOI	***2.66***	***3.30***	***1.78***	***1.25***	***2.58***	4.77	4.74	4.65	2.77	2.85	2.73
Mg#	***61.48***	***64.41***	***51.48***	***64.08***	***70.56***	55.80	55.80	53.70	49.70	50.3	50.10
DI	***23.65***	***21.28***	***33.63***	***25.14***	***28.9***	32.16	32.82	29.32	38.18	38.84	39.39
Traces (ppm)											
Cs	***0.38***	***0.57***	***0.48***	***0.47***	***0.55***	1.00	1.00	1.00	1.00	1.00	1.00
Rb	***37.44***	***42.48***	***53.31***	***42.81***	***48.81***	37.00	45.00	54.00	58.00	62.00	61.00
Ba	***491.75***	***708.48***	***648.23***	***713.95***	***684.35***	881.00	950.00	990.00	1111.00	979.00	975.00
Sr	***944.17***	***894.01***	***1340.06***	***1093.67***	***1018.6***	1230	1213.00	1377.00	889.00	1401	797.00
Pb	***3.17***	***3.62***	***4.59***	***3.66***	***3.73***	7.00	7.00	25.00	29.00	33.00	32.00
Th	***7.54***	***7.87***	***10.30***	***8.18***	***8.10***	9.00	11.00	17.00	19.00	19.00	19.00
U	***1.96***	***1.97***	***2.77***	***2.05***	***1.92***	1.00	1.00	4.00	4.00	4.00	4.00
Zr	***330.5***	***288.05***	***530.02***	***286.76***	***232.26***	349.00	352.00	427.00	401.00	348.00	339.00
Hf	***7.36***	***6.21***	***11.15***	***6.20***	***4.96***	6.00	6.00	8.00	8.00	8.00	8.00
Ta	***6.01***	***5.67***	***8.12***	***5.68***	***5.13***	3.00	3.00	8.00	8.00	8.00	8.00
Y	***27.8***	***26.08***	***34.38***	***25.13***	***20.10***	23.00	31.00	34.00	37.00	40.00	35.00
Nb	***85.64***	***82.39***	***110.28***	***82.66***	***76.82***	89.00	92.00	151.00	142.00	133.00	137.00
Sc	***22.96***	***25.76***	***14.50***	***24.87***	***17.58***	22.00	24.00	16.00	13.00	14.00	14.00
Cr	***357.56***	***431.6***	***143.48***	***516.77***	***645.61***	179.00	188.00	120.00	121.00	118.00	119.00
Ni	***249.75***	***245.95***	***95.16***	***294.44***	***476.49***	169.00	175.00	110.00	93.00	105.00	103.00
Co	***53.58***	***53.27***	***40.69***	***53.67***	***54.62***	29.00	38.00	46.00	44.00	45.00	39.00
V	***235.8***	***214.98***	***175.43***	***211.28***	***182.31***	221.00	219.00	225.00	224.00	222.00	219.00
W	***2.36***	***2.19***	***1.89***	***3.12***	***2.61***	1.00	1.00	2.00	2.00	2.00	1.00
Ga	***20.15***	***18.24***	***25.61***	***18.63***	***17.18***	22.00	29.00	22.00	26.00	28.00	24.00
Zn	***119.29***	***111.84***	***173.8***	***110.40***	***97.84***	109.00	118.00	130.00	131.00	113.00	116.00
Cu	***38.46***	***46.90***	***24.22***	***46.96***	***38.84***	26.00	37.00	40.00	60.00	58.00	56.00
La	***60.94***	***61.44***	***87.25***	***60.84***	***60.27***	77.00	89.00	125.00	130.00	133.00	131.00
Ce	***122.45***	***120.48***	***175.05***	***118.92***	***110.56***	160.00	164.00	222.00	221.00	226.00	231.00
Pr	***14.14***	***13.72***	***20.35***	***13.39***	***11.76***	10.00	10.00	23.00	23.00	23.00	22.00
Nd	***55.31***	***53.90***	***80.30***	***52.13***	***43.75***	67.00	70.00	83.00	82.00	79.00	77.00
Sm	***10.85***	***10.21***	***15.48***	***9.84***	***7.69***	7.00	8.00	14.00	14.00	15.00	15.00
Eu	***3.41***	***3.20***	***4.75***	***3.07***	***2.42***	2.00	2.00	4.00	4.00	4.00	4.00
Gd	***8.82***	***8.01***	***11.85***	***7.75***	***6.07***	7.00	7.00	11.00	10.00	10.00	11.00
Tb	***1.20***	***1.08***	***1.57***	***1.05***	***0.82***	1.00	1.00	1.00	2.00	2.00	2.00
Dy	***6.28***	***5.78***	***8.03***	***5.63***	***4.40***	5.00	5.00	8.00	8.00	8.00	7.00
Ho	***1.13***	***1.04***	***1.38***	***1.01***	***0.79***	1.00	2.00	1.00	1.00	1.00	1.00
Er	***2.62***	***2.44***	***3.10***	***2.39***	***1.87***	2.00	3.00	3.00	3.00	3.00	3.00
Tm	***0.34***	***0.33***	***0.39***	***0.32***	***0.25***	0.00	0.00	0.00	0.00	0.00	0.00
Yb	***2.00***	***1.92***	***2.27***	***1.88***	***1.47***	3.00	3.00	2.00	2.00	3.00	3.00
Lu	***0.28***	***0.27***	***0.31***	***0.27***	***0.22***	0.00	0.00	0.00	0.00	0.00	0.00
Eu/Eu*	***1.06***	***1.08***	***1.07***	***1.07***	***1.08***	0.87	0.82	0.98	1.03	1.00	0.95
Norm CIPW											
Orthose	***8.55***	***10.00***	***12.19***	***10.54***	***9.44***	8.09	8.40	-	13.99	14.67	13.98
Albite	***5.99***	***5.33***	***11.94***	***5.18***	***13.8***	17.45	18.13	-	7.44	5.91	10.72
Anorthite	***19.69***	***20.83***	***17.84***	***17.79***	***18.44***	20.44	18.77	7.88	9.32	8.44	9.40
Leucite	-	-	-	-	-	-	-	9.96	-	-	-
Nepheline	***9.11***	***5.95***	***9.50***	***9.42***	***5.66***	6.61	6.29	19.36	16.76	18.27	14.69
Diopside	***23.87***	***25.45***	***17.12***	***25.03***	***16.01***	19.19	20.58	35.76	23.95	24.71	22.21
Larnite	-	-	-	-	-	-	-	2.08	-	-	-
Olivine	***21.20***	***22.19***	***18.09***	***22.02***	***27.98***	17.12	16.54	12.95	16.24	15.70	16.74
Magnetite	***2.39***	***2.26***	***2.51***	***2.26***	***2.00***	2.21	2.21	2.54	2.58	2.53	2.56
Ilmenite	***6.97***	***5.74***	***7.31***	***5.55***	***4.95***	6.03	6.11	6.05	6.26	6.29	6.25
Apatite	***2.24***	***2.25***	***3.52***	***2.21***	***1.72***	2.85	2.97	3.41	3.48	3.50	3.45
$^{87}Sr/^{86}Sr$		***0.70312***	***0.70299***	***0.70321***	***0.70305***						
$2\sigma.10^{-6}$		***5.00***	***5.00***	***5.00***	***4.00***						
$^{143}Nd/^{144}Nd$		***0.512891***	***0.512927***	***0.512867***	***0.512862***						
$2\sigma.10^{-6}$		***4.00***	***4.00***	***4.00***	***3.00***						
$^{145}Sm/^{144}Sm$		***0.348404***	***0.348413***	***0.348415***	***0.348407***						
$2\sigma.10^{-6}$		***3.00***	***3.00***	***3.00***	***2.00***						
$^{87}Rb/^{86}Rb$		***0.133446***	***0.109633***	***0.109929***	***0.134577***						
$^{147}Sm/^{144}Sm$		***0.110572***	***0.112502***	***0.110136***	***0.102566***						
$(^{87}Sr/^{86}Sr)Ma$		***0.703116***	***0.702987***	***0.703206***	***0.703051***						
$(^{143}Nd/^{144}Nd)Ma$		***0.512888***	***0.512924***	***0.512864***	***0.512859***						
$^{147}Sm/^{144}Sm$		***0.110572***	***0.112502***	***0.110136***	***0.102566***						
εNdi		***5.11***	***5.81***	***4.64***	***4.54***						

Table 5 (end)

Rock type	Basalt									Latite
Sample	**PK1**	**PK30**	**WA5**	**WA3**	**WA2**	**WA8**	**WA6**	**WA1**	**BA16**	**BJM 59A**
SiO_2	43.09	42.82	46.17	47.69	48.01	47.61	47.79	47.88	46.66	***55.39***
TiO_2	2.97	3.00	2.30	2.48	2.42	2.46	2.44	2.41	2.17	***1.60***
Al_2O_3	12.99	13.69	13.36	14.39	14.4	14.39	14.43	14.33	15.95	***15.41***
Fe_2O_3	12.19	11.99	10.25	10.55	10.68	10.79	10.66	10.59	11.21	***9.14***
MnO	0.21	0.19	0.16	0.18	0.13	0.15	0.15	0.17	0.16	***0.15***
MgO	7.66	7.63	9.69	9.14	9.13	9.16	9.11	9.12	5.29	***3.49***
CaO	9.98	9.79	10.10	9.06	9.02	9.06	9.01	9.11	6.88	***5.65***
Na_2O	3.32	3.29	2.85	2.99	2.86	2.85	2.87	2.83	2.77	***3.21***
K_2O	1.42	1.33	1.64	1.77	1.65	1.80	1.81	1.80	1.34	***3.42***
P_2O_5	1.13	1.15	0.49	0.55	0.61	0.58	0.57	0.59	0.54	***0.47***
TOTAL (wt.%)	**94.96**	**94.88**	**97.01**	**98.8**	**98.91**	**98.85**	**98.84**	**98.83**	**92.97**	***97.93***
LOI	4.71	4.70	2.82	1.05	1.09	1.01	1.16	1.06	6.81	***1.32***
Mg#	55.50	55.80	65.20	63.20	62.90	62.70	62.90	63.10	48.30	***43.07***
DI	32.98	32.65	31.53	35.19	34.65	34.71	35.10	34.94	34.09	***53.57***
Traces (ppm)										
Cs	1.00	1.00	1.00	0.00	0.00	1.00	1.00	0.00	1.10	***2.61***
Rb	33.00	41.00	40.00	36.00	33.00	38.00	38.00	42.00	59.00	***148***
Ba	862.00	941.00	881.00	7.99.00	820.00	833.00	841.00	829.00	1023.00	***648.47***
Sr	1220.00	1191.00	701.00	746.00	742.00	751.00	722.00	732.00	1332.00	***396.92***
Pb	14.00	9.00	22.00	20.00	25.00	19.00	22.00	23.00	39.00	***14.64***
Th	11.00	11.00	5.00	6.00	6.00	5.00	3.00	6.00	19.00	***14.06***
U	1.00	1.00	2.00	2.00	2.00	2.00	2.00	2.00	4.10	***1.94***
Zr	353.00	331.00	260.00	265.00	249.00	255.00	271.00	266.00	359.00	***390.81***
Hf	6.00	6.00	6.00	6.00	6.00	6.00	6.00	5.00	8.20	***9.44***
Ta	3.00	3.00	4.00	4.00	3.00	3.00	3.00	3.00	8.50	***2.04***
Y	29.00	33.00	30.00	21.00	21.00	26.00	28.00	26.00	35.00	***47.33***
Nb	91.00	95.00	66.00	59.00	66.00	64.00	56.00	69.00	89.00	***22.37***
Sc	27.00	31.00	21.00	19.00	22.00	22.00	19.00	21.00	14.00	***17.18***
Cr	167.00	159.00	424.00	427.00	404.00	422.00	422.00	419.00	120.00	***169.96***
Ni	177.00	168.00	405.00	417.00	422.00	399.00	411.00	417.00	101.00	***41.05***
Co	25.00	35.00	40.00	45.00	47.00	48.00	51.00	44.00	44.00	***25.87***
V	218.00	220.00	190.00	177.00	169.00	181.00	179.00	180.00	221.00	***107.57***
W	2.00	1.00	1.00	2.00	1.00	1.00	1.00	1.00	1.00	***7.58***
Ga	30.00	27.00	15.00	19.00	21.00	15.00	18.00	18.00	22.00	***24.13***
Zn	114.00	122.00	88.00	8.00	94.00	101.00	94.00	92.00	100.00	***109.00***
Cu	31.00	33.00	55.00	62.00	59.00	60.00	62.00	61.00	40.00	***21.02***
La	88.00	76.00	49.00	48.00	48.00	39.00	48.00	44.00	121.00	***54.31***
Ce	155.00	161.00	88.00	93.00	93.00	94.00	90.00	90.00	233.00	***118.36***
Pr	10.00	10.00	11.00	10.00	10.00	10.00	10.00	10.00	22.9.00	***13.87***
Nd	59.00	70.00	41.00	40.00	40.00	41.00	39.00	40.00	77.00	***53.42***
Sm	8.00	7.00	7.00	8.00	8.00	8.00	7.00	7.00	13.00	***10.77***
Eu	2.00	2.00	2.00	2.00	2.00	2.00	2.00	2.00	4.29	***2.29***
Gd	7.00	7.00	7.00	7.00	7.00	6.00	7.00	7.00	11.50	***9.32***
Tb	1.00	2.00	1.00	1.00	2.00	1.00	1.00	1.00	1.00	***1.43***
Dy	4.00	5.00	5.00	5.00	5.00	5.00	5.00	5.00	8.10	***8.69***
Ho	1.00	2.00	1.00	1.00	1.00	2.00	1.00	1.00	1.20	***1.79***
Er	2.00	2.00	2.00	2.00	2.00	2.00	2.00	3.00	3.30	***4.82***
Tm	0.00	0.00	0.00	0.00	0.00	0.00	0.00	0.00	0.42	***0.73***
Yb	3.00	3.00	2.00	2.00	2.00	2.00	2.00	2.00	2.40	***4.67***
Lu	0.00	0.00	0.00	0.00	0.00	0.00	0.00	0.00	0.33	***0.70***
Eu/Eu*	0.82	0.87	0.87	0.82	0.82	0.88	0.87	0.87	1.07	***0.70***
Norm CIPW										
Quartz	-	-	-	-	-	-	-	-	-	***4.82***
Orthose	8.94	8.38	10.08	10.69	9.95	10.87	10.93	10.87	8.61	***20.8***
Albite	17.10	17.89	17.14	22.92	24.70	22.91	23.43	23.62	25.48	***27.94***
Anorthite	17.41	19.89	19.58	21.06	22.03	21.61	21.60	21.53	29.49	***18.07***
Nepheline	6.95	6.38	4.31	1.59	-	0.94	0.75	0.45	-	*-*
Diopside	22.38	19.44	23.57	17.12	15.83	16.52	16.37	16.73	3.11	***6.35***
Wollastonite	0.00	-	-	-	0.00	-	-	-	-	*-*
Hypersthene	-	-	-	-	1.01	-	-	-	24.25	***16.14***
Olivine	16.19	16.91	17.76	18.65	18.47	19.12	18.97	18.86	1.11	*-*
Magnetite	2.24	2.21	1.84	1.86	1.88	1.90	1.88	1.87	2.11	***1.63***
Ilmenite	6.01	6.07	4.55	4.81	4.69	4.77	4.73	4.68	4.48	***3.12***
Corindon	-	-	-	-	-	-	-	0.00	-	-
Apatite	2.79	2.84	1.18	1.30	1.44	1.37	1.35	1.40	1.36	***1.12***

Table 6: Whole rock chemical analyses of the studied mantle xenoliths

Rock type	Lherzolite					
Sample	**BIW 88E**	**BIW 88-2**	**BIW 88-1**	**BIW 88-3**	**BIW 88-5**	**BIW 88-4**
SiO_2	45.23	44.62	43.83	44.29	45.33	41.08
Al_2O_3	3.31	3.87	3.29	2.13	3.30	1.38
Fe_2O_3	8.55	8.98	9.05	8.72	8.87	9.02
MgO	34.61	34.54	34.02	39.23	37.51	39.70
CaO	4.18	4.65	5.10	3.17	2.81	4.31
Na_2O	0.22	0.24	0.26	0.20	0.22	0.14
K_2O	0.07	0.10	0.16	0.06	0.04	0.05
TiO_2	0.09	0.08	0.08	0.11	0.07	0.08
P_2O_5	< L.D.	< L.D.	< L.D.	< L.D.	< L.D.	< L.D.
MnO	0.12	0.13	0.12	0.12	0.13	0.13
LOI	2.99	2.44	3.37	1.11	1.08	3.06
Total (wt%)	99.37	99.65	99.28	99.14	99.35	98.95
Mg#	88.90	88.40	88.20	89.90	89.30	89.70
Trace (ppm)						
Cs	0.07	0.08	0.08	0.05	0.05	0.06
Rb	6.48	7.94	12.11	4.78	3.49	4.12
Ba	8.90	10.90	8.78	< L.D.	7.13	7.67
Sr	84.62	70.41	76.40	52.00	13.95	182.35
Pb	0.51	< L.D.	< L.D.	< L.D.	< L.D.	< L.D.
Th	0.10	0.10	0.04	0.05	0.15	0.12
U	0.04	0.07	0.06	0.03	0.06	0.07
Zr	6.03	1.63	2.99	9.30	4.47	6.78
Hf	0.14	0.08	0.09	0.23	0.08	0.15
Ta	0.07	0.01	0.01	0.03	0.03	0.07
Y	2.41	2.63	2.40	2.40	2.37	1.68
Nb	1.92	0.40	0.44	0.56	0.73	1.29
Sc	15.26	17.47	15.47	13.04	15.69	9.42
Cr	2910.95	2980.16	3020.06	2500.54	2804.73	1459.50
Ni	1867.04	1725.95	1919.51	2115.29	1878.44	2372.31
Co	99.57	98.79	105.34	105.82	103.47	118.56
V	69.36	83.74	70.880	52.13	66.92	37.41
W	3.85	3.40	4.48	5.18	5.46	4.28
Ga	3.02	3.49	2.94	2.42	2.83	1.39
Zn	56.03	58.85	56.60	50.93	52.14	52.78
Cu	16.85	21.56	24.66	7.98	19.06	8.52
As	< L.D.	< L.D.	0.51	< L.D.	0.749	0.67
Cd	0.05	0.03	0.05	0.09	0.03	0.03
Ge	0.80	0.91	0.78	0.82	0.81	0.73
Mo	5.01	4.63	6.07	7.91	8.93	5.49
Sb	0.16	0.22	0.12	0.08	0.15	0.14
Sn	0.45	< L.D.	0.36	< L.D.	0.41	0.33
Ta	0.07	0.01	0.01	0.03	0.03	0.07
La	0.86	1.25	0.72	0.90	0.79	0.81
Ce	1.49	1.37	0.71	2.45	0.90	1.67
Pr	0.18	0.11	0.07	0.38	0.08	0.20
Nd	0.74	0.38	0.32	1.79	0.32	0.84
Sm	0.20	0.15	0.13	0.45	0.13	0.21
Eu	0.08	0.07	0.06	0.16	0.05	0.08
Gd	0.27	0.26	0.24	0.45	0.21	0.24
Tb	0.05	0.06	0.05	0.07	0.05	0.04
Dy	0.39	0.44	0.39	0.45	0.36	0.29
Ho	0.09	0.11	0.10	0.09	0.09	0.07
Er	0.27	0.31	0.28	0.25	0.28	0.17
Tm	0.04	0.05	0.05	0.04	0.05	0.03
Yb	0.30	0.34	0.31	0.24	0.32	0.19
Lu	0.05	0.05	0.05	0.04	0.05	0.03
Eu/Eu*	1.06	1.01	1.02	1.06	0.97	1.08

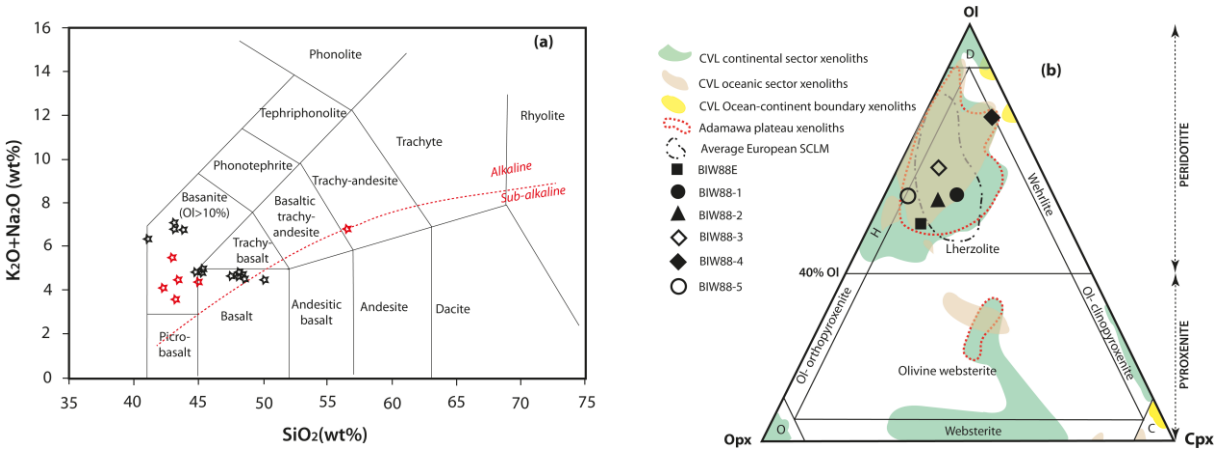

Figure 4: Nomenclature of the studied rocks samples. a) Position of Bini Warack lavas in the Na_2O+K_2O vs SiO_2 classification diagram of LeBas et al. (1986) – The black stars correspond to data from Tiabou et al. (2019) while the red stars are analyses from the current work; b) Position of the studied mantle xenoliths in the classification diagram for ultramafic rocks of Streckeisen (1976) compared to other mantle xenoliths studied along the CVL. Ol = olivine; Opx = orthopyroxene; Cpx = clinopyroxene; D = dunite; O = orthopyroxenite; C = clinopyroxenite; H= Harzburgite. Average European subcontinental lithospheric mantle (AESCLM) after Downes (1997); xenoliths from respective sectors of the CVL modified from Pinter et al. (2015) using recent data of Nkouandou et al. (2015), Wagsong Njombie et al. (2018), Tedonkenfack et al. (2021) and Puziewicz et al. (2023).

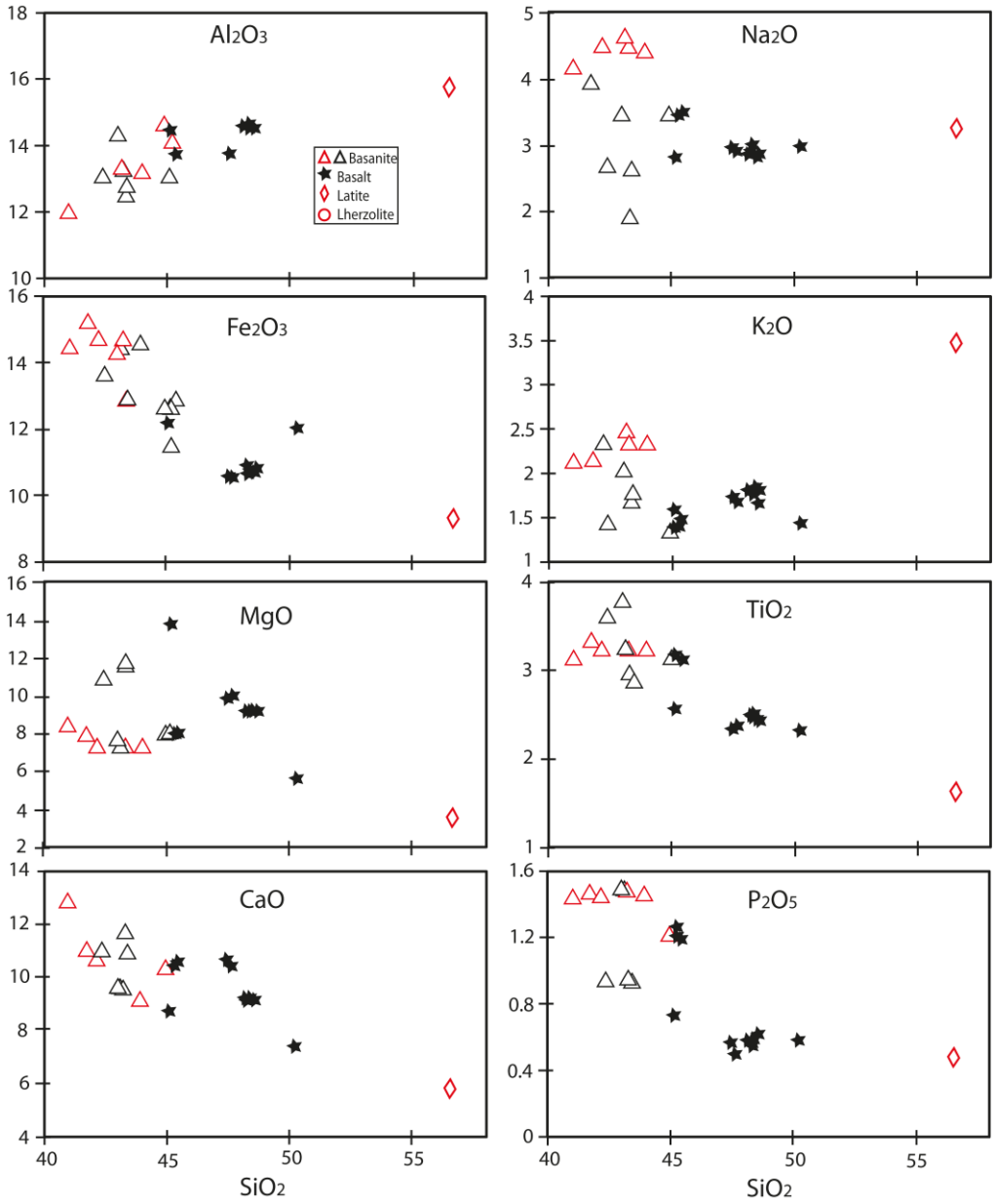

Figure 5: Harker diagrams of host lavas. The legend is the same as in figure 3. The same rock types from Tiabou et al. (2019) are represented in black color.

Trace elements

The amounts of some trace elements vary significantly from mafic to felsic lavas. Ni (41.05 – 476.5 ppm with the highest value in the basanite MBA11), Cr (6 – 645 ppm with the highest value in MBA11); Cu (≤ 60 ppm with maximum in basalts WA3 and WA6), Co (25 – 55 ppm with highest amount in MBA11), Nb (22.4 – 151 with highest value in basanite BA19), Zn (8 – 174 ppm with the highest value in basanite SAF88), Y (20 – 47 ppm) with the highest value

in BJM59A), Ga (15 – 28 ppm with highest value in BA50) and Pb (3 – 39 ppm with highest value in basalt BA16). The amounts of incompatible trace elements range from 397 to 1401 ppm for Sr, 492 to 1111 ppm for Ba, 232 to 530 ppm for Zr, 5 to 11 ppm for Hf and 2 to 8.5 ppmfor Ta. The ranges of some compatible trace elements contents such as Co, Ni, Cr, V, Sc, Cu and Zn are consistent with fractional crystallization. The Co and Ni contents are lower than those for primitive magmas (Co: 50 – 70 ppm; Ni: 300 – 400 ppm; Tatsumi et al., 1983, Jung & Masberg, 1998) and are therefore strongly in support of prior fractionation of olivine. The distribution of selected trace elements relative to SiO_2 contents displays no significant correlation.

The Chondrite–normalized multi–element diagrams (see Fig. 7a–c) are comparable with those of oceanic island basalts (OIB) and show enrichment in Ba, Th, U, Nb and La. The basanites and basalts spectra exhibit all a negative anomalies in K, Ti and Y while latite displays negative anomalies in K, Nb and Ti. The chondrite normalized rare earth elements (REE) patterns of lavas are quite homogeneous (see Fig. 7b–d). They show a strong enrichment in LREEs compared with HREEs reflected by moderate to high $(La/Yb)_N$ ratio (9.3 – 30). The mafic lavas show an overall weak positive Eu anomaly, contrary to latite displaying a negative one. The values of Eu anomalies [$Eu/Eu^*=Eu_N/(Sm_N\ Gd_N)^{1/2}$] as defined by Taylor & McLennan (1985) range from 1.08 – 0.82 in mafic lavas to 0.70 in latite.

4.3.2 Lherzolites

Whole–rock compositions

According to their modal compositions determined using MINSQ program (Herrmann & Berry, 2002), the analyzed Bini Warack mantle xenoliths are all lherzolites (see Fig. 4b). They are enriched in Al_2O_3 (1.38 – 3.87 wt%), CaO (2.81–5.1 wt%), TiO_2 (0.07 – 0.11 wt%), and Na_2O (0.14 – 0.26 wt%) relative to harzburgite from the southern Dibi area (Al_2O_3: 0.8 – 1.3 wt%, CaO: 0.32 – 1.4 wt%, TiO_2: 0.06 - 0.21 wt%, and Na_2O: 0.08 –0.26 wt%; Cf. Adama et al., 2021). Their bulk-rock Mg# ranges from 88.2 to 89.9 and comparable with that of their olivine (Mg#: 84.4 – 91), and Opx (Mg#: 89.7 – 90.92). They are similar in terms of bulk-rock

composition with the estimated primitive mantle (see McDonough & Rudnick, 1998) and the neighbouring Youkou volcano lherzolites (Wagson Njombié et al., 2018). Given their position in the whole rock compositional variation in Al_2O_3 vs. CaO diagram (Fig. 6) the studied peridotites evidenced low partial-melting degrees (<15%).

Their primitive mantle normalized REE patterns enable to distinguish two types of lherzolites:1/ those displaying spoon-shaped REE patterns (e.g: BIW88-1, BIW88-2, BIW88-5) with inflection at Nd or Sm, depending on the sample, marked by enrichment in LREEs and HREEs (0.7 – 5.6 times C1) relative to MREEs: $[La/Sm]_N$ = 2.51 – 5.24, $[Sm/Yb]_N$ = 0.44 – 1.25, and $[La/Yb]_N$ = 1.70 – 3.15 and 2) the lherzolite BIW88-3 displaying a more or less "S-shaped" REE pattern (Fig. 7h) characterized by LREEs enrichment over MREEs and HREEs. Their chondrite normalized multi-elements spider diagrams are marked by somewhat slightly higher contents in LILE relative to HFSE, with positive anomalies in Rb, K and Sr (Fig. 7g).

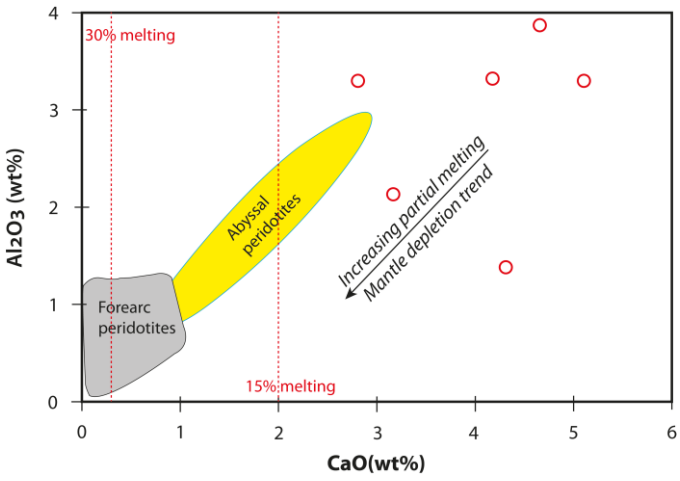

Figure 6: Whole-rock compositional variation in Al_2O_3 vs. CaO diagram. Forearc and abyssal peridotites fields are after Ishii et al., 1992; Pearce et al., 1992 respectively.

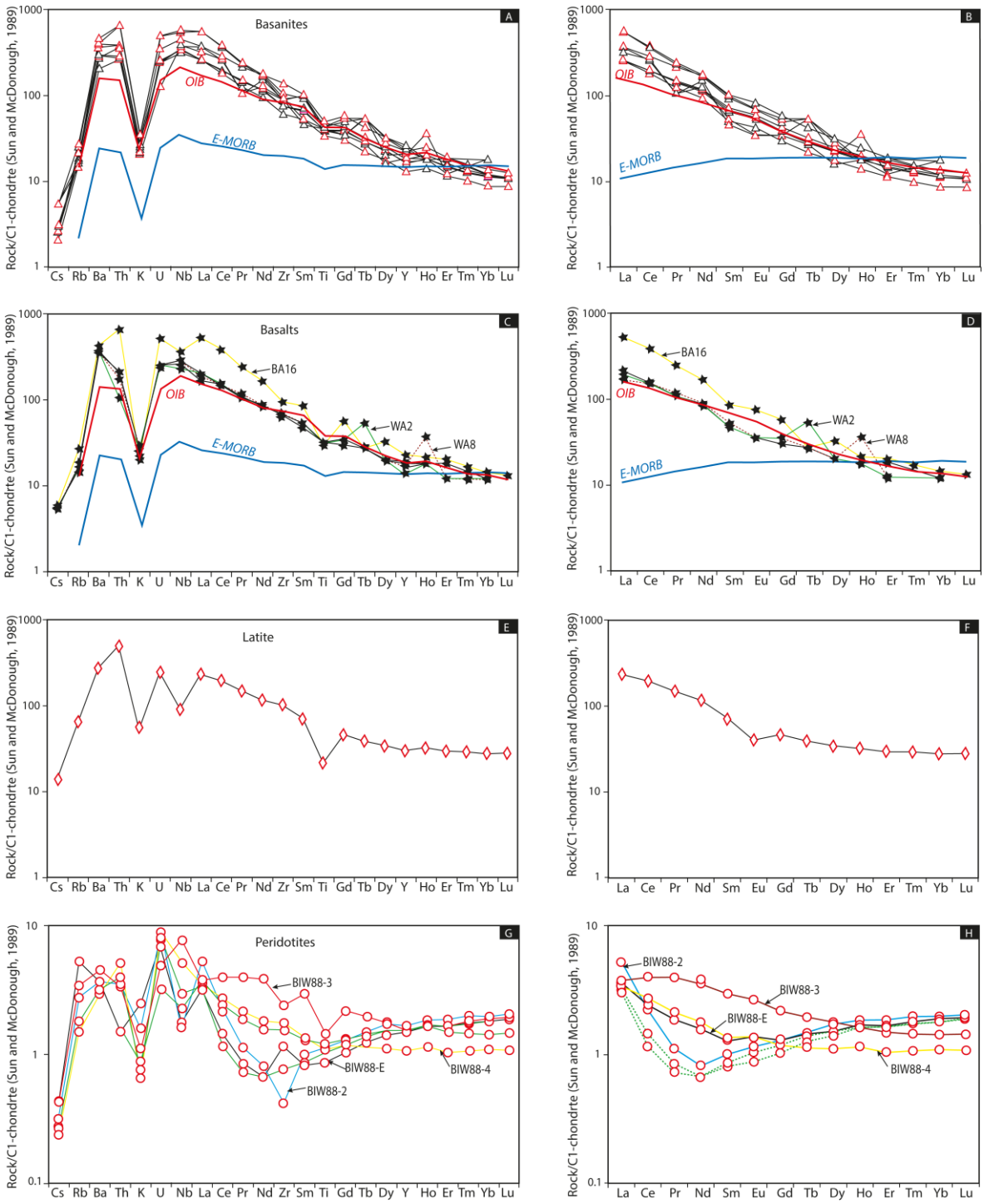

Figure 7: Chondrite-normalized multi-elements and rare earth elements diagrams of Bini Warack lavas and hosted mantle xenoliths. In red color are samples from this study while samples from Tiabou et al. (2019) are in black; OIB and E-MORB data are from Sun and McDonough (1989).

4.4 Nd and Sr isotopic signatures

Four new Rb/Sr and Sm/Nd isotopic ratios were obtained in mafic host lavas. They are characterized by $^{87}Sr/^{86}Sr$ isotopic ratios ranging between 0.702994 (basanite SAF88) and 0.703213 (basanite SOT22), $^{143}Nd/^{144}Nd$ from 0.512862 (basanite MBA11) to 0.512927 (basanite SAF88), with low $^{87}Rb/^{86}Sr$ ratios (< 0.15) and low $^{147}Sm/^{144}Nd$ ratios (0.10 – 0.11). The measured isotopic data have been corrected to 11.39 Ma representing the oldest dated lava in the area (Marzoli et al., 1999) in order to compare them to the available data from Miocene lavas along the CVL. The analyzed samples are characterized by initial $^{87}Sr/^{86}Sr_{(11.39\ Ma)}$ between 0.702987 and 0.703206 and initial $^{143}Nd/^{144}Nd_{(11.39\ Ma)}$ between 0.512854 and 0.512918. The selected analyzed samples display positive $\varepsilon Nd_{(11.39\ Ma)}$ ranging from +4.84 to +6.09.

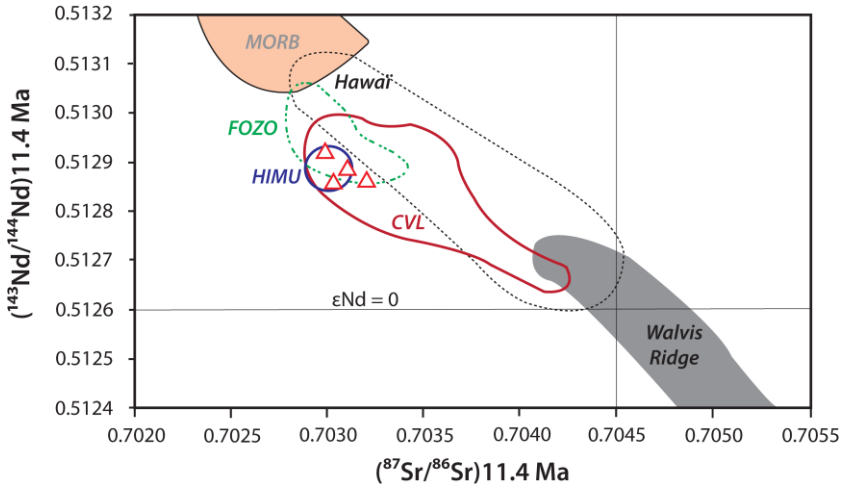

Figure 8: Plot of the Bini Warack lavas isotopic data in $(^{87}Sr/^{86}Sr)_{initial}$ vs. $(^{143}Nd/^{144}Nd)_{initial}$ diagram. The MORB, HIMU, and FOZO mantle poles are from Zindler and Hart (1986); the Walvis and Hawaii fields are from Aït Hamou et al., 2000; the CVL lava fields are from Halliday et al. (1990) and Marzoli et al. (2000).

5. Discussion

5.1 Characteristics of the SCLM beneath Bini Warack area

At first glance, the low Sr isotopic ratios (0.70299 – 0.70312) coupled with the positive initial εNd of the Bini Warack host lavas, refer to their mantle origin. However, due to the fact that

we did not carry out isotopic measurements on all the samples, we will invoke other criteria to constrain their mantle source characteristics.

5.1.1 Magmas sources and nature of the SCLM beneath the Adamawa Plateau

The bulk rock geochemical data of the Bini Warack host lavas all plot above the ΔNb line in the Nb/Y and Zr/Y ratio diagram (Fig. 9a), thus pointing out their compatibility with a mantle plume activity. The OIB affinity of the Bini Warack host lavas illustrated above by the similarities of the rare earth and multi-element spectra, as well as the strong involvement of the HIMU-like signature in their genesis are also highlighted in the $(^{87}Sr/^{86}Sr)_{initial}$ vs. $(^{143}Nd/^{144}Nd)_{initial}$ diagram (see Fig. 8).

Considering that Mn has high affinity for garnet and that Al content is very sensitive to temperature, De Hoog et al. (2010) used these major elements in olivine to define mantle lithologies and therefore to distinguish between garnet peridotite, spinel peridotite and garnet-spinel peridotite. The olivine in the studied xenoliths and xenocrysts displays low Al contents (average Al_2O_3 = 0.03 wt%), and high Mn contents (average MnO = 0.14 wt%) similar to those of spinel–lherzolite, showing that the lithology of the mantle lithosphere beneath Bini Warack is likely spinel lherzolite, which is consistent with geochemical findings (Fig. 9b).

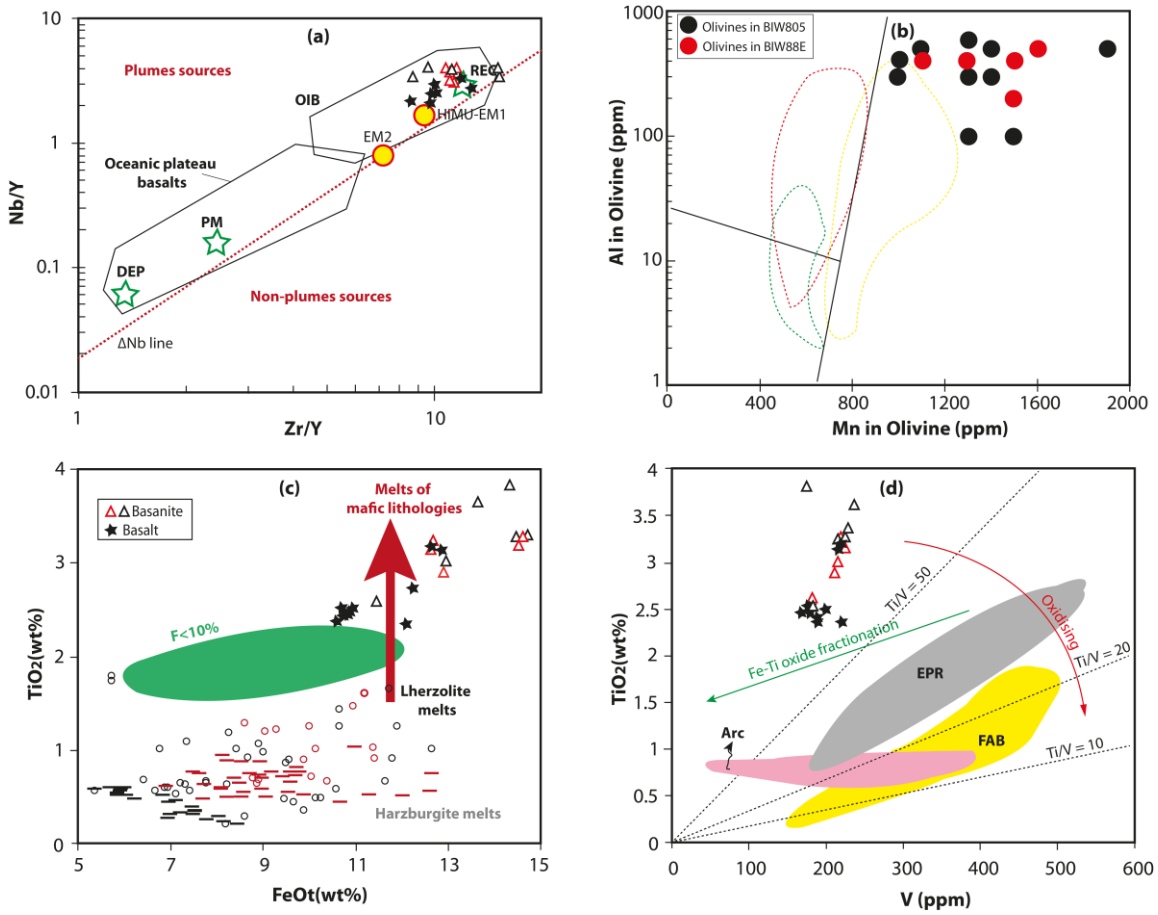

Figure 9: (a) Plot of the host lavas relative to various mantle compositional components (green star) and fields for basalts from different tectonic settings as defined by Weaver (1991) and Condie (2005); (b) Plot of Al vs. Mn for the olivine xenocrysts; (c) Comparison of Bini Warack basanites and basalts with experimental melts of representative mantle lithologies using their TiO_2 and FeO_t contents; (d) TiO_2 vs. V plot of Bini basanites and basalts. In (a) DEP=deep depleted mantle; EM1= enriched mantle sources; HIMU= high U/Pb mantle source; OIB=oceanic island basalt; PM= primitive mantle; REC= recycled component. In (b) the fields of spinel–garnet lherzolite (dashed green line), garnet–lherzolite (dashed red line) and the spinel–lherzolite (yellow line) are after Yuan & Yan (2022). The green ellipse in (c) denotes the low–degree (<10%) experimental melts of fertile lherzolite. The black circles illustrate partial melts of fertile lherzolite while the red ones highlight experimental melt formed at 1.5 – 2.5 GPa; just as the black dashes represent the composition of harzburgite partial melts and the red ones that of their experimental melt at 1.5 – 2.5 GPa. The thick red arrow schematically shows non-

peridotite mantle rocks (e.g., amphibolite, silica-deficient and silica-excess pyroxenites) typically with high TiO_2 contents (≥ 2 wt%; Kushiro, 1996). Data for experimental melts of lherzolite and harzburgite are consistent with the compilation of Dai et al. (2023). In (d) the compositional zones for volcanic rocks from various tectonic settings and the magmatic differentiation trend caused by Fe-Ti oxides fractionation are from Reagan et al. (2010). FAB= Fore arc basalts; EPR = East Pacific Rise.

5.1.2 Thickness, volume and thermal evolution of the SCLM reservoir beneath Bini Warack

Olivine is one of the major rock-forming minerals in peridotite, and its Fo values are generally considered as a proxy for the extent of partial melting (Pearson, 1999). Forsterite values in the studied mantle xenoliths range from 84 to 91%. This Fo range is typical of olivine of the mantle xenoliths of the Ngaoundéré area (89 – 91%: Nkouandou et al., 2015; Nkouandou & Temdjim, 2011; Wagsong Njombié et al., 2018) and similar both to that of off-craton mantle rocks (88 – 92%: Boyd & Mertzman 1987; Boyd et al. 1997) and oceanic mantle residues (90.5 – 91.5%: Boyd, 1989) indicating that the SCLM beneath the Bini Warack region is likely juvenile and comparable to the oceanic lithospheric mantle.

Generally, the iron content of the residue, unlike the magnesium content, is sensitive to melting pressure (Herzberg, 2004). Therefore, Mg# in whole rocks, in combination with Al_2O_3, can help to infer the melting depth (Herzberg & Rudnick, 2012). The FeOt, Al_2O_3 and MgO contents of the Bini Warack peridotites suggest that their melting began at depths ≤ 2 GPa, similar to those of the harzburgite xenoliths from the nearby Guinadji Djalsoka and Mokolo-Kapsiki localities (Fig. 10a-b). Due to their sensitivity to pressure variations, elements such as the REE, Ti, Na, and Hf are proxy to constrain melting depths (Putirka, 1999). The remarkable negative K peak contrary to Ba in the multi-element profiles (see Fig. 7), indicates the presence of hydrous mineral phases such as plogopite and amphibole in the mantle source.

On the other hand, melts in equilibrium with amphibole-bearing source would have rather low Rb/Sr (<0.1) and higher Ba/Rb (>20), while melts being produced with phlogopite in the source would inherit low Ba/Rb values (Furman and Graham, 1999; Ma et al., 2014). Therefore, the low Rb/Sr (0.03 – 0.37) and high Ba/Rb (4.4 – 26) ratios of the host lavas from Bini Warack are reliable with the presence of amphibole in the source region. These two hydrous minerals are known to be stable at depths less than 150 km. Furthermore, the presence of sharp contacts of mantle xenoliths with the host lavas may indicate that the magma hosting these mantle materials was likely produced at about 80 to 150 km within the garnet peridotite mantle stability field as it was evidenced for mantle xenoliths from Oku volcanic group by Asaah et al. (2015a). Those depths values estimated from geochemical data and mineralogical evidences are consistent with geophysical estimates. Indeed, the deepest density discontinuity so far determined beneath the Adamawa region using spectral analysis of gravity data ranges between 75 and 149 km, and corresponds to an anomalous low velocity upper mantle structure (Nnangue et al., 2000). On the other hand the Moho discontinuity depth ranges from 19 to 36 km (Fairhead & Okereke, 1988, Poudjom Djomani, 1995, Nnange et al., 2000, Tokam et al., 2010), depending on the methods used. These depths overall evidence a crustal thinning related to a mantle upwelling process similar to that described for the northern Kapsiki plateau (Tamen et al., 2015).

The Bini Warack mantle xenoliths are characterized by protogranular to porphyroclastic textures. The work of Zangana et al. (1997) demonstrated that undeformed mantle xenoliths, i.e. those showing protogranular to porphyroclastic textures such as those from Bini Warack, have high equilibrium temperatures (> 900 °C) contrary to deformed xenoliths which have lower equilibrium temperatures (< 900 °C).

The pyroxene equilibrium temperatures estimated using the geothermometers of Brey & Kohler (1990) and Liang et al. (2013), and also taking into account the Cr# ratios of the spinel in lherzolites, vary from 900 to 1100 °C. This equilibrium temperature gradient is identical to that of the mantle xenoliths of the OVG lavas (Puziewicz et al., 2023) located approximately 300 km SW of our study area along the CVL.

5.2 Melting conditions for magmas generation

It is noteworthy that partial melts derived from refractory harzburgites are characterized by low TiO_2 contents (< 1 wt%; Falloon & Danyushevsky, 2000), while melts derived from mafic lithologies (various types of pyroxenites, hornblendite, etc.) typically have high TiO_2 contents (> 2 wt%; e.g., Kushiro, 1996). The basaltic rocks from Bini Warack area that have high TiO_2 contents could rightly be considered, referring to Dai et al. (2023), as issued from the partial melting of silica–deficient pyroxenites embedded in a fertile lherzolitic mantle. Their TiO_2 contents are higher than those of harzburgite-derived melts but similar to those of non-peridotite mantle lithologies and those of low-extent melts derived from low degree (< 10%) of melting of fertile lherzolites (Fig. 9c). Besides their high TiO_2 contents they display high Ti/V ratios, suggestive of low oxygen fugacity (Fig. 9d).

The presence of garnet in the mantle source is sustained by the overall enrichment in LREE and MREE relative to HREE (see Fig. 7h). The Zr/Nb vs. La/Yb diagram (Fig. 10a) allows estimating both the amount of garnet in the source and the degree of melting. Thus, it appears that the basalts from Bini Warack definitely fit in the area of alkali basalts of the CVL, and are derived from < 2% partial melting of a lherzolitic mantle source, containing 2 to 6% of garnet, such as alkaline basalts from the OVG studied by Asaah et al. (2015a). In the Yb/Sm vs. Tb/Yb diagram (Fig. 10b), the studied mafic lavas from Bini Warack area lie on the mixing paths of low-extent (<10%) melts from spinel- and garnet-facies mantle sources. As the basaltic rocks of the northwest China craton (Dai et al., 2024), the basaltic lavas from Bini Warack area tend to cluster at low Tb/Yb ratios. This is thought to be related to negligeable amount of garnet peridotite-derived melt fractions relative to that of the spinel peridotite-derived melt fraction in the studied basaltic rocks.

Given that heavy REE are sensitive to the presence of garnet during melting, their bulk-rock abundance combined with residue/melt partitioning modeling, are likely to constrain the melting pressure (Canil, 2004, Simon et al., 2008). Fig. 10c-d display the range of whole–rock REE models of the Bini Warack lherzolite samples together with modeling results for the composition of melt residues that start melting within the spinel and garnet stability field from

a fertile mantle source with a depleted MORB mantle composition (Workman & Hart, 2005). In the melting model within the spinel stability field, the degree of melt extraction for the Bini Warack mantle xenoliths would be somewhat ≥10%, similar to the melting estimates of major elements (see Fig. 10e-f). On the other hand, their HREE contents (e.g: Yb) are consistent with a low degree (≤ 4 %) of polybaric melting that starts in the garnet stability field and ends in the spinel stability field (Fig. 10e), simulating the ascent of mantle plumes (Simon et al., 2008, Doucet et al., 2012).

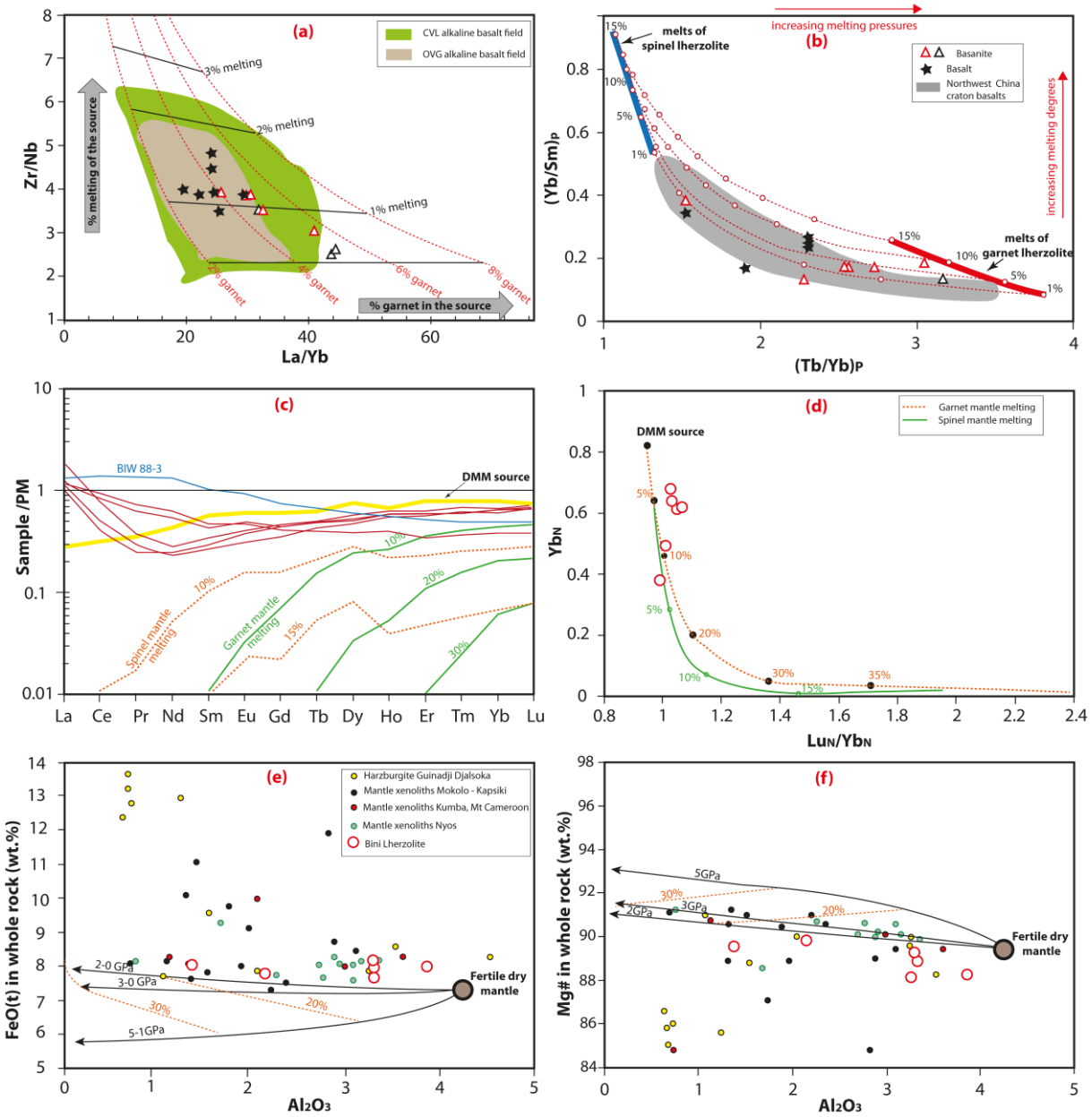

Figure 10: Co-variation diagrams of major, trace and rare earth elements. (a) Modeled melting (Zr/Nb vs. La/Yb) results for the studied mafic lavas together with other mafic lavas

687 with MgO>4 from the OVG and CVL. Melts that produced most basanites and alkali basalts
688 were produced by <2% partial melting of a dominantly garnet (<6%) bearing mantle
689 lherzolite. (b) Estimate of the melting degrees of the Bini mafic lavas, given a fertile lherzolite
690 source with primitive mantle-like trace-element contents (McDonough & Sun, 1995). The
691 dashed red lines designate the mixing paths of aggregated fractional partial melts from
692 garnet- and spinel-facies lherzolites at the fixed melting degrees (1%, 5%, 10%, 15%).
693 Partition coefficients are taken from Bédard (2006) for olivine, orthopyroxene, clinopyroxene
694 and spinel, and from Adam & Green (2006) for garnet. In black color are samples from
695 Tiabou et al. (2019). (c) Primitive mantle (McDonough & Sun, 1995) normalized REE for the
696 Bini lherzolites. The trace element modeling results for mantle melting in spinel and garnet
697 stability fields of a fertile mantle source, and that of the depleted MORB mantle source
698 (DMM) (Workman & Hart, 2005) (modeling of Doucet et al., 2023) are also shown. (d)
699 Lu_N/Yb_N vs. Yb_N for Bini lherzolites compared to melting model in spinel stability field (green
700 line) and garnet stability field (red dashed line). The primitive mantle values are from
701 McDonough & Sun (1995). Trace element modeling for a DMM source in spinel and garnet
702 stability fields with garnet exhaustion after 20% of melting. (e) and (f) Whole rock Al_2O_3 vs
703 Mg# and FeO_t of the studied lherzolite together with other mantle xenoliths from northern
704 Cameroon. The composition of Northwest China craton basalts are from Dai et al. (2024),
705 and that of mantle xenoliths from Nyos (Bilong et al., 2010; Teitchou et al., 2011), Kumba
706 after Sababa et al. (2015), Mt. Cameroon after Wandji et al. (2009), Mokolo (ongoing work),
707 Kapsiki after Tamen et al. (2015), Guinnadji and Djalsoka after Adama et al. (2021). Thick
708 black lines show the compositions for melting residue formed by isobaric batch melting of
709 fertile mantle source at 2, 3 and 5 GPa (Herzberg, 2004). Dashed red lines show polybaric
710 melt extraction at 20% and 30% of melting.
711
712 **5.3 Assimilation and fractional crystallization (AFC)**
713 In general, magmas rising from mantle are possibly contaminated by assimilation of crustal
714 material, depending on the time taken to reach the surface. The presence of mantle xenoliths

715 in most of our studied lavas is indicative of a rapid ascent of their parental magmas, which
716 does not favor extensive fractional crystallization and substantial contamination in crustal
717 magma chambers. Nb/Ta ratios for the majority of Bini Warack lavas vary between 10 and 19
718 with an average of 15 and do not vary meaningfully with SiO_2 (Fig.11a), pointing out their
719 genetic relationship and their evolution by fractional crystallization. These values are similar
720 for the entire CVL (average Nb/Ta = 16: Asaah et al., 2015b). The relatively low Sr isotopic
721 compositions of the analyzed basanites (< 0.704) preclude any consistent crustal
722 contamination. Moreover, the plot of the Bini Warack lavas in the AFC modeling diagram of
723 DePaolo, 1981 (Fig. 11b) reveals that almost all plot around the initial magma composition
724 and out of AFC curves. This indicates a small amount of fractional crystallization and
725 insignificant assimilation, except for the latite sample which is the most evolved lava
726 displaying high Rb/Zr ratio.
727 Major and trace elements compositions of the Bini Warack mafic lavas (Table 5) such as Ni
728 (89 – 477 ppm), Cr (104 – 646 ppm), Co (25 – 55 ppm) and MgO contents (Mg# ≤ 71) are
729 not so different from those of primary magmas in equilibrium with mantle olivine as defined
730 by Jung & Masberg (1998) and Frey et al., 1978; (Ni: 300 – 500 ppm; Cr: 300 – 500 ppm;
731 Co: 50 – 70 ppm and Mg#: 68 – 72) and infer the slight incidence of fractional crystallization.
732 Basanite samples have Mg# ≥61 and high Ni (209 – 476.5 ppm) and Cr (340 – 645.6 ppm)
733 contents, nearly matching with those of primary magmas. The decrease of CaO with
734 increasing SiO_2 contents in the Bini Warack lavas provides evidence for the fractional
735 crystallization of both olivine and clinopyroxene. Conversely, the constant positive correlation
736 of Al_2O_3 with SiO_2 observed in the studied lavas, point out that the crystallization of
737 plagioclase was very restricted during their differentiation.

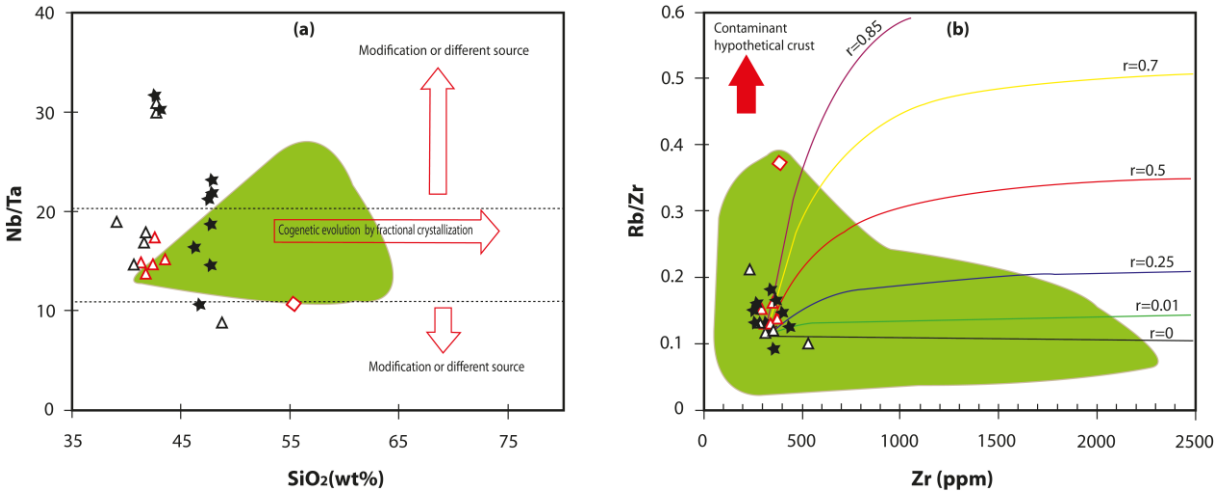

Figure 11. Plot of Bini Warack lavas in (a) the Nb/Ta vs. SiO_2 diagram illustrating the narrow variation of Nb/Ta ratios for most samples; (b) AFC Rb/Zr vs. Zr Modeled diagram. The green field represents CVL lavas (Asaah et al., 2015b). The legend is the same as in the previous figure.

5.4 Mantle metasomatism

The presence of clinopyroxene associated with secondary olivine and spinels confirm that this metasomatism took place in asthenospheric upwelling settings (e.g. Grégoire et al., 2000 a-b, Moine et al., 2001, Delpech et al., 2004).

Trace elements such as LILE and HFSE are frequently used to constrain the metasomatic nature and conditions (e.g., Xu et al., 2022), in basaltic rocks. Modal metasomatism is generally evidenced in mantle xenoliths by the presence of mineral phases such as amphibole and phlogopite, while the effects of cryptic metasomatism are particularly noticeable by whole rock spectra and Cpx, enriched in LREE (Cvetkovic et al., 2022). The likely presence of amphibole and phlogopite as demonstrated in the preceding section is suggestive of the involvement of a metasomatized SCLM.

According to Pearce (2008), the inference regarding hydrous metasomatism can be further evidenced by the Nb/Yb vs. Th/Yb diagrams. In this diagram, the mafic lavas from Bini Warack overlap the mantle array defined by oceanic basalts, except for a few samples with markedly elevated Th/Yb at given Nb/Yb (Fig. 12a). This agrees well with the fact that

759 metasomatic agents are generally controlled by H_2O-bearing melts/fluids, which have a low
760 capacity to mobilize elements such as Th, Nb, and Yb (Johnson & Plank, 1999). As shown in
761 Fig. 12a, the basaltic lavas from the Bini Warack area display greater Th/Yb relative to the
762 mantle array (but somewhat similar with those of recent basalts from the North China
763 Craton), archetypal of lavas originated from the lithospheric mantle metasomatized by partial
764 melts derived from subducted continental crust (Zhang et al., 2002).
765 According to Furman & Graham (1999), partial melts derived from amphibole- and
766 phlogopite-bearing mantle sources are characterized by high Rb/Sr and Ba/Sr ratios,
767 respectively. Mafic lavas (basanite + basalt) from Bini Warack overall exhibit high Ba/Rb
768 (12.2 – 26.1) and low Rb/Sr (0.03 – 0.08) ratios (Fig. 12b), likely suggesting that
769 metasomatism by aqueous fluids may have triggered amphibole formation in the melt
770 sources. Admittedly, Dai et al. (2019) attributes the concurent presence of high Ba/Rb and
771 low Rb/Sr ratios to the legacy of subducted igneous oceanic crust; however, this latter
772 hypothesis cannot be considered given the continental intraplate setting of the lavas studied,
773 unless it's considered as a recycled ancient oceanic crust.
774 The olivine crystals presented in this study have high Ca/Fe and 100*Mn/Fe ratios and low
775 100*Ni/Mg ratio (Fig. 12c-d), symptomatic of olivine crystallization from a carbonated mantle
776 source-derived magmas according to Ammannati et al. (2016). In other words, the SCLM
777 beneath the Bini Warack area have undergone a carbonate metasomatism.

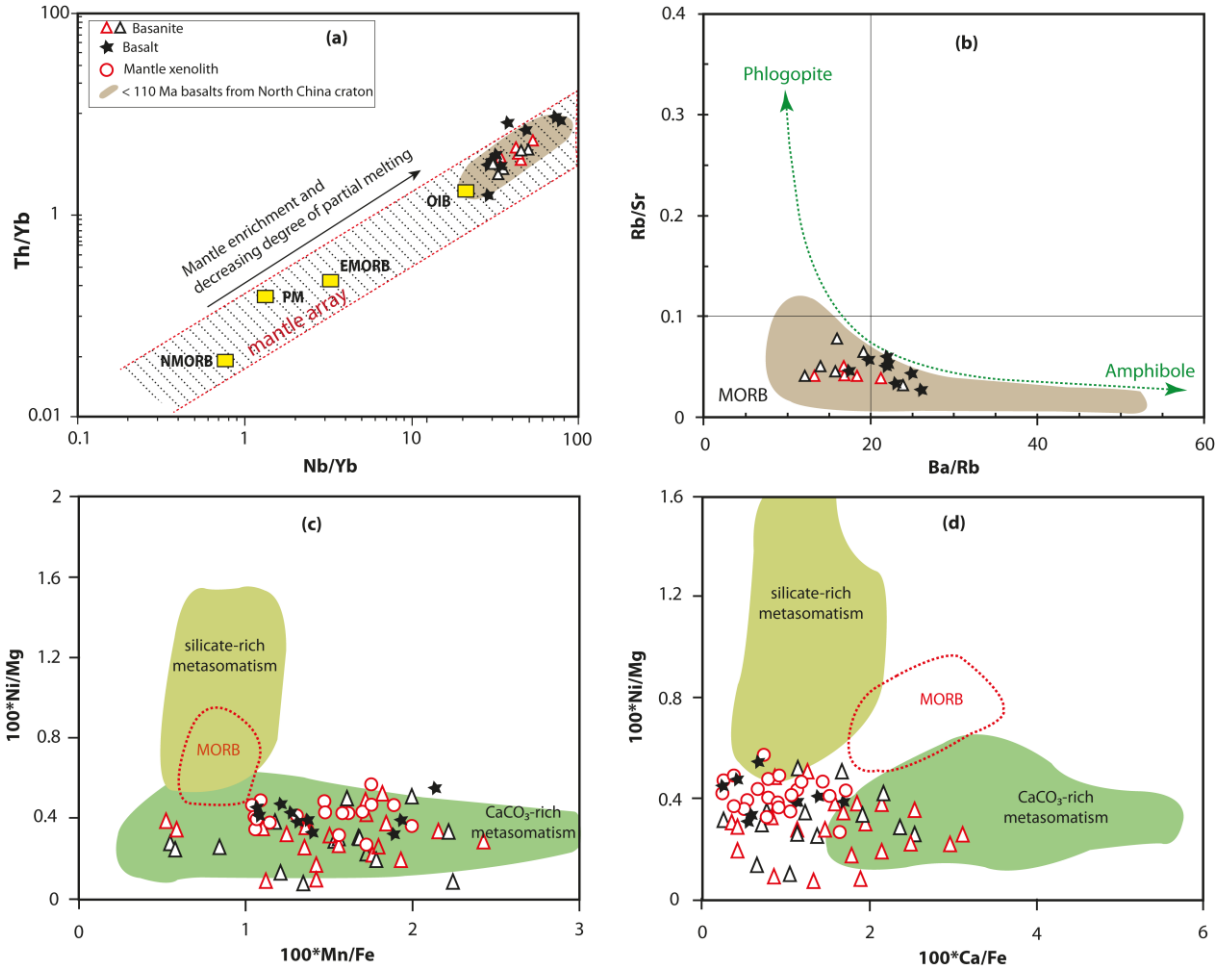

Figure 12: Plots of bulk rock (a) Th/Yb vs. Nb/Yb, (b) Rb/Sr vs. Ba/Rb, (c) olivines 100*Mn/Fe vs. 100*Ni/Mg, and (d) 100*Ca/Fe vs. 100*Ni/Mg. The mantle array in (a) is defined by oceanic basaltic rocks and the vertical black arrows indicate the effect of crustal melt input in the source of basaltic rocks (Pearce, 2008). In (b), the arrows showing partial melts from amphibole- and phlogopite-bearing mantle sources are adopted from Furman & Graham (1999). The compositions of MORB are taken from Gale et al. (2013). The olivine data for MORB are from Sobolev et al. (2007).

Conclusion

The present mineralogical and geochemical study of lavas and hosted xenoliths from Bini Warack area of the CVL shed light on magmatic events, petrogenetic processes and provides informations on the sub–continental mantle beneath the Adamawa plateau, marking

the transition from the Congo Archean-Paleoproterozoic craton to the Neoproterozoic juvenile crust involved in the Pan-African Central Africa Orogenic Belt.

Lavas from Bini Warack are alkaline and include basanite, alkali basalt and latite, with SiO_2 contents ranging from 42.4 to 56.6 wt% while mantle xenoliths are all spinel bearing lherzolite with protogranular to porphyroclastic textures. Mafic lavas are sodic while the only latite sample is potassic, both originated from a similar mantle source with signatures of at least three mantle components (REC, HIMU and EM1). Their OIB character and isotopic ratios are consistent with plume activity.

The mantle xenoliths are spinel lherzolites displaying protogranular to porphyroclastic textures, mainly consisting of minerals with fertile compositions (Fo_{84-91}, spinel Cr#:0.1 – 0.22; Al–rich pyroxenes), and are characterized by U/Th typically lower than 1, as well as slight enrichment in LILE relative to HFSE.

The presence of mantle xenoliths in most lavas and the relatively low Sr isotopic of the latter indicate a rapid ascend of their parental magmas, low degree of fractional crystallization and insignificant assimilation or crustal contamination. According to the melting model, the parental magmas of the studied lavas were generated near 80 to 150 km depth, by ≤ 2% partial melting of lherzolitic mantle source containing 2–6% of garnet, and characterized by a low oxygen fugacity condition and low water content. Trace element concentrations together with olivines chemical features suggest that the SCLM beneath the Bini Warack area have undergone a carbonate–rich metasomatism.

Acknowledgments

The current work was financially supported by the CNRS– IRD LithoCOAC project. Two research stays in the laboratory *Geosciences Environnement Toulouse* of the University Paul Sabatier Toulouse 3, France, were consecutively granted to the first author for analytical facilities, in addition to his participation to the 2023 South America Exploration Initiative (SAXI) workshop in *Vallées d'Antraigues–Asperjoc* funded by the CNRS IRN FALCoL directed by Olivier Vanderhaeghe. We deeply acknowledge Fabienne De Parseval for the confection of the thin sections presented in this paper, and Philippe De Parseval, Sophie Gouy and Stéphanie Mandrou for their technical assistance during the microprobe and TIMS

analyses respectively. We also thank Etienne Médard and an anonymous reviewer for their significant and constructive comments, and the editorial assistance from Laurent Jolivet.

References

Adama H, Nkouandou OF, Bardintzeff JM, et al. 2021. Petrography and geochemistry of the harzburgite xenoliths of lake Guinnadji and Ngao Djalsoka volcano from the Dibi area (Adamawa Plateau – Cameroon). J Geogr Envir Earth Sci Intern 25 (10): 178–193.

Adam J, Green T. 2006. Trace element partitioning between mica- and amphibole-bearing garnet lherzolite and hydrous basanitic melt: 1.Experimental results and the investigation of controls on partitioning behaviour. Contrib Mineral Petrol 152: 1–17

Aït-Hamou F, Dautria J-M, Cantagrel J-M, Dostal J, Briqueu L. 2000. Nouvelles données géochronologiques et isotopiques sur le volcanisme cénozoïque de l'Ahaggar (Sahara algérien): des arguments en faveur de l'existence d'un panache. CR Acad Sci 330 (12): 829–836

Ammannati E, Jacob DE, Avanzinelli R, Foley SF, Conticelli S. 2016. Low Ni olivine in silica-undersaturated ultrapotassic igneous rocks as evidence for carbonate metasomatism in the mantle. Earth Planet Sci Lett 444: 64–74

Arai S. 1994. Characterization of spinel peridotites by olivine-spinel compositional relationships: Review and interpretation. Chem Geol 113 (3–4): 191–204

Asaah ANE, Yokoyama T, Aka TF, et al. 2015a. Geochemistry of lavas from maar–bearing volcanoes in the Oku volcanic group of the Cameroon Volcanic Line. Chem Geol 406: 55–69.

Asaah ANE, Yokoyama T, Aka TF, et al. 2015b. A comparative review of petrogenetic processes beneath the Cameroon Volcanic Line: Geochemical constraints. Geosci Frontiers 6 (4): 557-570

Bian X, Su Y, Zheng J, Wang J, Chen X, Zhou L, Dong B, and Niu T 2024**.** Multistage melt/fluid modification of lithospheric mantle beneath the circum-cratonic orogenic belt: Evidence from the Tuoyun peridotite xenoliths. Geol Soc America Bull, https://doi.org/10.1130/B37552.1.

Bardintzeff J-M, Nkouandou OF, Mefire AF. 2020. First occurrence of pigeonite in the Cameroon Volcanic Line. Arab J Geosci 13: 496

Bédard JH. 2006. A catalytic delamination-driven model for coupled genesis of Archaean crust and sub-continental lithospheric mantle. Geochim Cosmochim Acta 70: 1188–1214

Bénard A, Müntener O, Pilet S, Arculus R, Nebel O. 2021. Silica-rich spinel harzburgite residues formed by fractional hybridization-melting of the intra-oceanic supra-subduction zone mantle: new evidence from TUBAF seamount peridotites. Geochim Cosmochim Acta 293: 477–506

Bilong P, Ndjigui P-D, Temdjim R, Sababa E. 2011. Geochemistry of peridotite and granite xenoliths under the early stages of weathering in the Nyos volcanic region (NW-Cameroon): implications for PGE exploration. Chem Erde Geochem 71: 77–86

Boyd FR. 1989. Compositional distinction between oceanic and cratonic lithosphere: Earth Planet Sci Lett 1–2 (96): 15–26

Boyd FR, Mertzman SA. Composition and structure of the Kaapvaal lithosphere, Southern Africa. In: Mysen BO. (Ed.), Magmatic processes: physicochemical principles. Geochem Soc Houston, 1987, pp. 3–12

Boyd FR, Pokhilenko NP, Pearson DG, Mertzman SA, Sobolev NV, Finger LW. 1997. Composition of the Siberian cratonic mantle: Evidence from Udachnaya peridotite xenoliths: Contrib Min Petrol 2–3 (128): 228–246

Brey GP, Köhler T. 1990. Geothermobarometry in four phase lherzolites II. New thermobarometers and practical assessment of existing thermobarometers. J Petrol 31: 1353–1378

Caldeira R, Munhá JM. 2002. Petrology of ultramafic nodules from São Tomé Island, Cameroon Volcanic Line (oceanic sector). J Afr Earth Sci 34: 231–246

Canil D. 2004. Mildly incompatible elements in peridotites and the origins of mantle lithosphere. Lithos 77: 375–393

Carignan J, Hild P, Mevelle G, Morel J, Yeghicheyan D. 2001. Routine analyses of trace elements in geological samples using flow injection and low pressure on–line liquid

878 chromatography coupled to ICP–MS: A study of geochemical reference materials BR,
879 DR–N, UB–N, AN–G and GH. Geostand Newslett 25: 187–198
880 Carlson RW, Pearson DG, James DE. 2005. Physical, chemical, and chronological
881 characteristics of continental mantle: Rev Geophys 43 (1): doi:10.1029/2004RG000156
882 Christiansen E H, 2009. Petromode. Faculty publications, Brigham Young University.
883 http://scholarsarchive.byu.edu/facpub/1334 - Provo
884 Condie KC. 2005. High field strength element ratios in Archean basalts: a window to evolving
885 sources of mantle plume. Lithos 79: 491–504
886 Cvetković V, Radivojević M, Prelević D, Toljić M, Turki SM. 2022. An insight into the
887 evolution of the lithospheric mantle of south Saharan metacraton: Mantle xenoliths from
888 Jabal Eghei Volcanic Complex, Libya. J Volc Geotherm Res 432: 107691.
889 Dai HK, Zheng JP, O'Reilly SY, et al. 2019. Langshan basalts record recycled Paleo-Asian
890 oceanic materials beneath the northwest North China Craton. Chem Geol 524: 88–103
891 Dai HK, Zheng JP, Xiong Q, Griffin WL, O'Reilly SY. 2023. Continental thermal blanketing
892 explains the compositional dichotomy of the diffuse basaltic province across central-
893 eastern Asia. Geophys Res Lett 50: e2023GL104951
894 Dai HK, Zheng J, Xiong Q, Hu L, Zhou X. 2024. Insight of enriched basalts into the nature
895 and evolution of mantle lithosphere beneath craton margins. Sci China Earth Sci 67:
896 https://doi.org/10.1007/s11430-024-1371-x
897 De Hoog JCM, Gall L, Cornell DH. 2010. Trace-element geochemistry of mantle olivine and
898 application to mantle petrogenesis and geothermobarometry: Chem Geol 1–4 (270): 196–
899 215
900 Delpech G, Grégoire M, O'Reilly SY, Cottin JY, Moine B, Michon G. 2004. Feldspar from
901 carbonate– rich metasomatism in the oceanic mantle under Kerguelen Islands (South
902 Indian Ocean). Lithos 75: 209–237
903 Déruelle B, Ngounouno I, Demaiffe D. 2007. The Cameroon Hot Line (CHL): a unique
904 example of active alkaline intraplate structure in both oceanic and continental
905 lithospheres. CR Geosci 339: 589–598

Doucet LS, Ionov DA, Golovin AV, Pokhilenko NP. 2012. Depth, degrees and tectonic settings of mantle melting during craton formation: inferences from major and trace element compositions of spinel harzburgite xenoliths from the Udachnaya kimberlite, Central Siberia. Earth Planet Sci Lett 359-360: 206–218

Doucet L, Li Z–X, Brennan D, et al. 2023. Precambrian history of the Pacific Mantle Domain: New constraints from Woodsreef and Port Macquarie serpentinized spinel harzburgites of the New England orogen, Australia. J Petrol 64: 1–24

Downes H. Shallow continental lithospheric mantle heterogeneity–petrological constraints. In: Fuchs K. Ed. Upper mantle heterogeneities from active and passive seismology. Kluwer Academic, Dodrecht, 1997, pp. 295 – 308

Downes H, Reichow MK, Mason PRD, Beard AD, Thirlwall MF. 2003. Mantle domains in the lithosphere beneath the French Massif Central: trace element and isotopic evidence from mantle clinopyroxenes. Geol 200: 71–87

Fairhead JD, Okereke CS. 1988. Depths to major density contrasts beneath the West African rift system in Nigeria and Cameroon based on the spectral analysis of gravity data. J Afr Earth Sci 7 (5/6): 769–777

Falloon TJ, Danyushevsky LV. 2000. Melting of refractory mantle at 1.5, 2, and 2.5 GPa under anhydrous and H_2O-undersaturated conditions: Implications for the petrogenesis of high-Ca boninites and the influence of subduction components on mantle melting. J Petrol 41: 257–283

Frey FA, Green DH, Roy SD. 1978. Integrated models of basalts petrogenesis: a study of quartz tholeiites to olivine melilites from South Eastern Australia utilizing geochemical and experimental petrological data. J Petrol 19: 463–513

Furman T, Graham D. 1999. Erosion of lithospheric mantle beneath the East African Rift system: Geochemical evidence from the Kivu volcanic province. Lithos 48: 237–262

Grégoire M, Moine BN, O'Reilly SY, Cottin JY, Giret A. 2000a. Trace element residence and partitioning in mantle xenoliths metasomatised by high alkaline silicate and carbonate-rich melts (Kerguelen Islands, Indian Ocean). J. Petrol. 41: 477–509

934 Grégoire M, Lorand J-P, O'Reilly S-Y, Cottin J-Y. 2000b. Armalcolite-bearing, Ti-rich
935 metasomatic assemblages in harzburgitic xenoliths from the Kerguelen Islands:
936 Implications for the oceanic mantle budget of high-field strength elements. Geochim
937 Cosmochim Acta 64: 673–694
938 Halliday AN, Davidson JP, Holden P, DeWolf C, Lee D-C, Fitton J.G. 1990. Trace element
939 fractionation in plumes and the origin of HIMU mantle beneath the Cameroon line. Nature,
940 347: 523–528.
941 Hawkesworth CJ, Erlank AJ, Marsh JS, Menzies MA, Calsteren P. Evolution of the
942 continental lithosphere: evidence from volcanics and xenoliths from southern Africa. In
943 Hawkesworth CJ, Norry MJ. Eds. Continental basalts and mantle xenoliths. Shiva
944 Publishing Ltd., Nantwitch, Cheshire, 1983, pp. 111–138
945 Herrmann W, Berry RF. 2002. MINSQ - a least squares spreadsheet method for calculating
946 mineral proportions from whole rock major element analyses. Geochem Expl Envir Anal 2**:**
947 361–368
948 Herzberg C. 2004. Geodynamic in formation in peridotite petrology. J Petrol 45: 2507–2530
949 Herzberg C, Rudnick R. 2012. Formation of cratonic lithosphere: an integrated thermal and
950 petrological model. Lithos 149: 4–15
951 Ishii T, Robinson PT, Maekawa H, Fiske R. 1992. Petrological studies of peridotites from
952 diapiric serpentinite seamounts in the Izu- Ogasawara-Mariana forearc, Leg 125.
953 Proceeding of the Ocean Drilling Program, Scientific Results 125: 445–485
954 Itiga Z, Bardintzeff JM, Wotchoko P, Wandji P, Bellon H. 2013. Tchabal Gangdaba massif in
955 the Cameroon Volcanic Line: a bimodal association. Arab J Geosci 7(11): 4641–4664
956 Johnson MC, Plank T. 1999. Dehydration and melting experiments constrain the fate of
957 subducted sediments. Geochem Geophys Geosyst 1: 1007
958 Jung S, Masberg P. 1998. Major and trace element systematics and isotope geochemistry of
959 Cenozoic mafic volcanic from the Vogelsberg (Central Germany): constraints on the origin
960 of continental alkaline and tholeiitic basalts and their mantle sources. J Volcanol
961 Geotherm Res 86: 151–177

962 Kamenetsky VS, Crawford AJ, Meffre S. 2001. Factors controlling chemistry of magmatic
963 spinel: an empirical study of associated olivine, Cr-spinel and melt inclusion from primitive
964 rocks. J Petrol 42: 655–671
965 Kushiro I. 1996. Partial melting of a fertile peridotite at high pressures: An experimental study
966 using aggregates of diamond. Geophys Monogr 95: 109–122
967 Kretz R, 1983. Symbols for rock-forming minerals. Am.Min. **68**: 277–279.
968 Labou I, Benoît M, Baratoux L, et al. 2020. Petrological and geochemical study of Birimian
969 ultramafic rocks within the West African Craton: Insights from Mako (Senegal) and
970 Loraboué (Burkina Faso) lherzolite/harzburgite/wehrlite associations. J Afr Earth Sci 162:
971 103677
972 Lee D-C, Halliday AN, Davies GR, Essene EJ, Fitton JG, Temdjim R. 1996. Melt enrichment
973 of shallow depleted mantle: a detailed petrological, trace element and isotopic study of
974 mantle-derived xenoliths and megacrysts from the Cameroon Line. J Petrol 37 (2): 415–
975 441
976 Liang Y, Sun C, Yao L. 2013. A REE in-two-pyroxene thermometer for mafic and ultramafic
977 rocks. Geochim Cosmochim Acta 102: 246–260
978 Li C–F, Li X–H, Li Q–L, Guoa J–H, Lia X–H. 2011. Directly determining $^{143}Nd/^{144}Nd$ isotope
979 ratios using thermal ionization mass spectrometry for geological samples without
980 separation of Sm–Nd. J Anal At Spectrom 26: 2012-2022
981 Li C–F, Li X–H, Li Q–L, Guoa J–H, Li X–H, Yanga Y–H. 2012. Rapid and precise
982 determination of Sr and Nd isotopic ratios in geological samples from the same filament
983 loading by thermal ionization mass spectrometry employing a single–step separation
984 scheme. Anal Chim Acta 727: 54–60
985 Lin A–B, Aulbach S, Zheng J–P, et al. 2022. Lithospheric mantle provinces and crust–mantle
986 decoupling beneath northeastern China: Insights from peridotite xenoliths. GSA Bull 0: 1–
987 19

988 Liu J, Scott JM, Martin CE, Pearson DG. 2015. The longevity of Archean mantle residues in
989 the convecting upper mantle and their role in young continent formation: Earth Planet Sci
990 Lett 424: 109–118
991 Lundstrom CC, Hoernle K, Gill J. 2003. U–series disequilibria in volcanic rocks from the
992 Canary Islands: plume versus lithosphere melting. Geochim Cosmochim Acta 67: 4153–
993 4177
994 Ma L, Jiang SY, Hofmann AW et al. 2014. Lithospheric and asthenospheric sources of
995 lamprophyres in the Jiaodong Peninsula: a consequence of rapid lithospheric thinning
996 beneath the North China Craton? Geochim Cosmochim Acta 124: 250–271
997 MacDonald R, Rogers NW, Fitton JG, Black S, Smith M. 2001. Plume–lithosphere
998 interactions in the generation of the basalts of the Kenya Rift, East Africa. J Petrol 42:
999 877–900
1000 Marzoli A, Renne PR, Piccirillo EM, et al. 1999. Silicic magmas from the continental
1001 Cameroon Volcanic Line (Oku, Bambouto and Ngaoundere): ^{40}Ar-^{39}Ar dates, petrology,
1002 Sr-Nd-O isotopes and their petrogenetic significance. Contrib Mineral Petrol 135: 133-150
1003 Marzoli A, Piccirillo EM, Renne PR, et al. 2000. The Cameroon Volcanic Line revisited:
1004 petrogenesis of continental basaltic magmas from lithospheric and asthenospheric mantle
1005 sources. J Petrol 41: 87–109
1006 Maury RC, Brousse R. 1978. Présence de pigeonite et d'orthopyroxène dans certaines laves
1007 du Massif central français: leur répartition et leur origine. Bull Soc Française de
1008 Minéralogie et Cristallographie 109: 10–21
1009 Mbassa BJ, Sole J, Dawai D, et al. 2025. New K–Ar data in the northeastern edge of the
1010 Adamawa-Yadé domain, Central African Pan-African Fold belt: shedding light on the
1011 transition age between convergent and divergent tectonic regimes. CR Geosci 357: 145-
1012 165
1013 McDonough WF, Rudnick RL. Mineralogy and composition of the upper mantle. In: Russell J,
1014 Hemley (Eds.), Reviews in Mineralogy 37, Ultrahigh–pressure mineralogy: physics and

chemistry of the Earth's deep Interior. Ribbe PH. Series Ed., Mineral Soc Amer Washington DC, 1998, pp. 139–164.

McKenzie DP, O'Nions RK. 1983. Mantle reservoirs and oceanic island basalts. Nature 301: 229–231

McKenzie DP, O'Nions RK. 1995. The source regions of ocean island basalts. J Petrol 36: 133–159

Milelli L, Fourel L, Jaupart C. 2012. A lithospheric instability origin for the Cameroon Volcanic Line. Earth Planet Sci Lett 335–336: 80–87

Moine BN, Grégoire M, O'Reilly SY, Sheppard SMF, Cottin JY. 2001. High field strength element (HFSE) fractionation in the upper mantle: evidence from amphibole-rich composite mantle xenoliths from the Kerguelen Islands (Indian Ocean). J Petrol 42: 2145–2167

Morimoto N, Fabriès J, Ferguson AK, et al. 1988. Nomenclature of pyroxenes. Am Mineral 73: 1123–1133

Ngako V, Affaton P, Nnangue JM, Njanko T. 2003. Pan-African tectonic evolution in central and southern Cameroon: transpression and transtension during sinistral shear movements. J Afr Earth Sci 36: 207–214

Nguihdama D, Chazot G, Kamgang P, Mbowou GIB, Ngounouno I. 2014. Spinel–bearing lherzolite xenoliths from Hosséré Garba (Likok, Adamawa–Cameroon): Mineral compositions and geothermobarometric implications. Intern J Geosci 5: 1435–1444

Nkouandou OF, Temdjim R. 2011. Petrology of spinel lherzolite xenoliths and host basaltic lava from Ngao Voglar volcano, Adamawa Massif (Cameroon Volcanic Line, West Africa): equilibrium conditions and mantle characteristics. J Geosci 56: 375–387

Nkouandou OF, Ngounouno I, Déruelle B, Ohnenstetter D, Montigny R, Demaiffe D. 2008. Petrology of the Mio–Pliocene volcanism to the North and East of Ngaoundéré (Adamawa, Cameroon). CR Geosci 340: 28–37

Nkouandou OF, Bardintzeff J–M, Fagny AM. 2015. Sub–continental lithospheric mantle structure beneath the Adamawa plateau inferred from the petrology of ultramafic xenoliths

1043 from Ngaoundéré (Adamawa plateau, Cameroon, Central Africa). J Afr Earth Sci 111: 26–
1044 40
1045 Nnange Metuk J, Ngako V, Fairhead JD, Ebinger CJ. 2000. Depths to density discontinuities
1046 beneath the Adamawa Plateau region, Central Africa, from spectral analyses of new and
1047 existing gravity data. J Afr Earth Sci 30 (4): 887–901
1048 Nono A, Déruelle B, Demaiffe D, Kambou R. 1994. Tchabal Nganha volcano in Adamawa
1049 (Cameroon): petrology of a continental alkaline series. J Volcanol Geotherm Res 60: 147–
1050 178
1051 Owona S, Mvondo Ondoa J, Ekodeck GE. 2013. Evidence of quartz, feldspar and amphibole
1052 crystal plastic deformations in the Palaeoproterozoic Nyong complex shear zones under
1053 amphibolite to granulite conditions (West Central African Fold Belt, SW Cameroon). J
1054 Geogr Geol 5 (3): 186–201
1055 Pearce JA. 2008. Geochemical fingerprinting of oceanic basalts with applications to ophiolite
1056 classification and the search for Archean oceanic crust. Lithos 100: 14–48
1057 Pearson DG. 1999. The age of continental roots: Lithos 48: 171–194
1058 Pearson DG, Nowell GM. 2002. The continental lithospheric mantle: characteristics and
1059 significance as a mantle reservoir. Phil Trans R Soc London A 360: 2383–2410
1060 Pearce JA, Van der Laan SR, Arculus RJ, et al. 1992. Boninite and harzburgite from Leg 125
1061 (Bonin-Mariana forearc): A case study of magma genesis during the initial stages of
1062 subduction. Proceeding of the Ocean Drilling Program, Scientific Results, 125: 623–659
1063 Pintér Z, Patkó L, Djoukam JFT, et al. 2015. Characterization of the sub–continental
1064 lithospheric mantle beneath the Cameroon volcanic line inferred from alkaline basalts
1065 hosted peridotite xenoliths from Barombi Mbo and Nyos Lakes. J Afr Earth Sci111: 170–
1066 193
1067 Poudjom Djomani Y, Nnange, MJ, Diament C, Ebinger, Fairhead J. 1995. Effective elastic
1068 thickness and crustal thickness variations in West Central Africa inferred from gravity
1069 data. J Geophys Res 100 (B11): 22047–22070.

1070 Puziewicz J, Aulbach S, Kaczmarek M–A, et al. 2023. The origin and evolution of DMM–like
1071 lithospheric mantle beneath continents: mantle xenoliths from the Oku volcanic group in
1072 the Cameroon Volcanic Line, West Africa. J Petrol 64: 1–25
1073 Rankenburg K, Lassiter J, Brey G. 2005. The role of continental crust and lithospheric mantle
1074 in the genesis of Cameroon Volcanic Line lavas: Constraints from isotopic variations in
1075 lavas and megacrysts from the Biu and Jos Plateaux. J Petrol 46: 169–190
1076 Reagan MK, Ishizuka O, Stern RJ, et al., 2010. Fore–arc basalts and subduction initiation in
1077 the Izu–Bonin–Mariana system. Geochem Geophys Geosyst 11: Q03X12
1078 Sababa E, Ndjigui P-D, Ebah Abeng SA, Bilong P. 2015. Geochemistry of peridotite xenoliths
1079 from the Kumba and Nyos areas (southern part of the Cameroon volcanic line):
1080 implications for Au-PGE exploration. J. Geochem Explor 152: 75–90
1081 Simon NSC, Neumann E-R, Bonadiman C, et al. 2008. Ultra-refractory domains in the
1082 oceanic mantle lithosphere sampled as mantle xenoliths at Ocean Islands. J Petrol 49:
1083 1223–1251
1084 Smith JV, Brown W. Nomenclature, General properties of feldspars and simple determinative
1085 diagrams. In: Feldspar Minerals: Second Revised and Extended Ed. Springer Verlag,
1086 Berlin Heidelberg, 1988, pp. 208-228
1087 Sobolev AV, Hofmann AW, Kuzmin AV, et al. 2007. The amount of recycled crust in sources
1088 of mantle-derived melts. Sci 5823 (316): 412–417
1089 Stevens RE. 1944. Composition of some chromites of the western hemisphere. Amer Mineral
1090 29: 1-34
1091 Stracke A, Hofmann AW, Hart SR. 2005. FOZO, HIMU, and the rest of the mantle zoo.
1092 Geochem Geophys Geosyst 6, Q05007, doi:10.1029/2004GC000824
1093 Streckeisen A. 1976. To each plutonic rock its proper name. Earth Sci Rev 12: 1–33
1094 Suh CE, Luhr JF, Njome MS. 2008. Olivine-hosted glass inclusions from Scoriae erupted in
1095 1954–2000 at Mt Cameroon volcano, West Africa. J Volcanol Geotherm Res 169: 1–33
1096 Tamen J, Nkoumbou C, Mouafo L, Reusser E, Tchoua FM. 2007. Petrology and
1097 geochemistry of monogenetic volcanoes of the Barombi Koto volcanic field (Kumba

graben, Cameroon volcanic line): Implications for mantle source characteristics. CR Geosci 339: 799–809

Tamen J, Nkoumbou C, Reusser E, Tchoua F. 2015. Petrology and geochemistry of mantle xenoliths from the Kapsiki Plateau (Cameroon Volcanic Line): Implications for lithospheric upwelling. J Afr Earth Sci 101: 119–134

Tatsumi YM, Sakuyama H, Fukuyama H, Kushiro I. 1983. Generation of basalt magmas and the thermal structure of the mantle wedge in subduction zones. J Geophys Res 88: 5815–5825

Tedonkenfack SST, Puziewicz J, Aulbach S, et al. 2021. Lithospheric mantle refertilization by DMM-derived melts beneath the Cameroon Volcanic Line – a case study of the Befang xenolith suite (Oku Volcanic Group, Cameroon). Contrib Mineral Petrol 176: 37, doi:10.1007/s00410–021–01796–3

Teitchou M.I, Grégoire M, Dantas C, Tchoua FM. 2007. Le manteau supérieur à l'aplomb de la plaine de Kumba (ligne du Cameroun), d'après les enclaves de péridotites à spinelles dans les laves basaltiques. CR Geosci 339: 101–109

Teitchou MI, Grégoire M, Temdjim R, Ghogomu RT, Ngwa C, Aka FT. 2011. Mineralogical and geochemical fingerprints of mantle metasomatism beneath Nyos volcano (Cameroon volcanic line). In: Beccaluva L, Bianchini G, Wilson M, Eds. Volcanism and Evolution of the African Lithosphere. Geol Soc Am Spec Paper 478: 193–210

Temdjim R, Njilah IK, Kamgang P, Nkoumbou C. 2004. Données nouvelles sur les laves felsiques de Ngaoundéré (Adamaoua, ligne du Cameroun): chronologie et pétrologie. Afr J Sci Technol 5(2): 113–123.

Temdjim R, Tchouankoué JP, Kamgang P, Tchoua F. 2006. Sur l'existence d'un maar trachytique dans la Ligne volcanique du Cameroun: le maar Mbalang–Djalingo dans la région de Ngaoundéré (Plateau de l'Adamaoua). Rev Géogr Cameroun XVII (1): 67–71

Thompson RN, Gibson SA. 2000. Transient high temperatures in mantle plume heads inferred from magnesian olivines in Phanerozoic picrites: Nature 407 (6803): 502–506

Tiabou FA, Temdjim R, Wandji P, et al. 2019. Baossi–Warack monogenetic volcanoes, Adamawa Plateau, Cameroon: petrography, mineralogy and geochemistry. Acta Geochim 38: 40 – 67

Tokam APK, Tabod CT, Nyblade AA, Julia J, Wiens DA, Pasyanos ME. 2010. Structure of the crust beneath Cameroon, West Africa, from the joint inversion of Rayleigh wave group velocities and receiver functions. Geophys J Int 183 (2): 1061–1076.

Wagsong Njombie MP, Temdjim R, Foley SF. 2018. Petrology of spinel lherzolite xenoliths from Youkou volcano, Adamawa massif, Cameroon Volcanic Line: mineralogical and geochemical fingerprints of sub–rift mantle processes. Contrib Mineral Petrol: 173, 13.

Weber B. 1991. Interactions between basalt and mantle lithosphere in intraplate oceanic context: examples from Tahiti and Tahaa (fast drifting plate) and Reunion island (slow drifting plate). Univ. thesis, Ecole des Mines de Paris, 222p. https://www.sudoc.fr/044195990

Workman RK, Hart SR. 2005. Major and trace element composition of the depleted MORB mantle (DMM). Earth Planet Sci Lett 231: 53–72

Xu R, Liu YS, Lambart S, et al. 2022. Decoupled Zn–Sr–Nd isotopic composition of continental intraplate basalts caused by two-stage melting process. Geochim Cosmochim Acta 326: 234– 252

Yokoyama T, Aka FT, Kusakabe M, Nakamura E. 2007. Plume–lithosphere interaction beneath Mt. Cameroon volcano, west Africa: constraints from ^{238}U–^{230}Th–^{226}Ra and Sr–Nd–Pb isotope systematics. Geochim Cosmochim Acta 71: 1835–1854

Yuan L, Yan Q. 2022. The nature of the sub–continental lithospheric mantle beneath Thailand: evidence from xenocrysts in Cenozoic basalts. Intern Geol Rev 65(3): 396-415.

Zangana NA, Downes H, Thirlwall MF, Hegner E, 1997. Relationship between deformation, equilibration temperatures, REE and radiogenic isotopes in mantle xenoliths Ray Pic, Massif Central, France: an example of plume–lithosphere interaction? Contrib Mineral Petrol 127: 187–203

1152 Zhang HF, Sun M, Zhou XH, Fan WM, Zhai MG, Yin JF. 2002. Mesozoic lithosphere
1153 destruction beneath the North China Craton: Evidence from major-, trace-element and Sr-
1154 Nd-Pb isotope studies of Fangcheng basalts. Contrib Mineral Petrol: 144: 241–254
1155 Zindler A. Hart SR. 1986. Chemical geodynamics. Annual Review of Earth Planetary Sci 14:
1156 493–571